Rheological Characterization of CNC-CTAB Network below and above the Critical Micelle Concentration (CMC)

by

Tina Raeisi Gahrooee

B.A., Azad University, Science and Research Tehran, 2017

MASc. Queen Mary University of London, 2018

A THESIS SUBMITTED IN PARTIAL FULFILLMENT OF

THE REQUIREMENTS FOR THE DEGREE OF

MASTER OF APPLIED SCIENCE

in

THE FACULTY OF GRADUATE AND POSTDOCTORAL STUDIES

(Chemical and Biological Engineering)

THE UNIVERSITY OF BRITISH COLUMBIA

(Vancouver)

December 2020

The following individuals certify that they have read, and recommend to the Faculty of Graduate and Postdoctoral Studies for acceptance, a thesis entitled:

Rheological characterization of CNC-CTAB network below and above the critical micelle concentration (CMC)

submitted by	Tina Raeisi Gahrooee	in partial fulfillment of the requirements for
the degree of	Master of Applied Science	
in	Chemical and Biological Engineering	

Examining Committee:

Dr. Savvas G. Hatzikiriakos, Chemical and Biological Engineering, UBC

Supervisor

Dr. Peter Englezos, Chemical and Biological Engineering, UBC

Supervisory Committee Member

Dr. Stavros Avramidis, Faculty of Forestry, UBC

Supervisory Committee Member

Abstract

The network of Cellulose Nanocrystal (CNC) suspension is explored below and above the critical micelle concentration (CMC), in the presence of cetyltrimethylammonium bromide (CTAB) with a positively charged head using rheological characterization. CNC-CTAB gel showed shear thinning behaviour, complex relationship between strain amplitudes and CTAB concentration, diminishing thixotropic behaviour as a function of CTAB and single and two yielding stress maxima as a function of CTAB, resulting from different microstructure below and above CMC of CTAB. Comparing the flow curves of CNC-CTAB suspension/gel revealed the role played by CTAB content, CNC concentration and sonication energy in strengthening of the network. We analysed and obtained yield stress from steady shear, creep testing and oscillatory experiments and compared them.

Lay Summary

Cellulose is a natural polymer that can be extracted from various sources such as plants, marine animals, algae, fungi, bacteria invertebrates, and amoeba. CNC, a product of hydrolysis of cellulose, can turn into a gel through introduction of a coagulant. Therefore, one aspect of CNC gel that needs proper attention is the investigation of its plurality of mechanical and rheological behaviour under various processing conditions. Therefore, the rheological behaviour of CNC-CTAB in suspension and gel formation, is studied in the presence of surfactants that gives rise to interesting rheological behaviour. The system studied in the present work is an attractive gel that displays tunable range of attraction and attraction strength due to charge screening of CTAB micelles (negatively charges) and CTAB molecule (positively charged head) length that is ~ 4nm. The system under study is viewed and studied from the colloidal perspective.

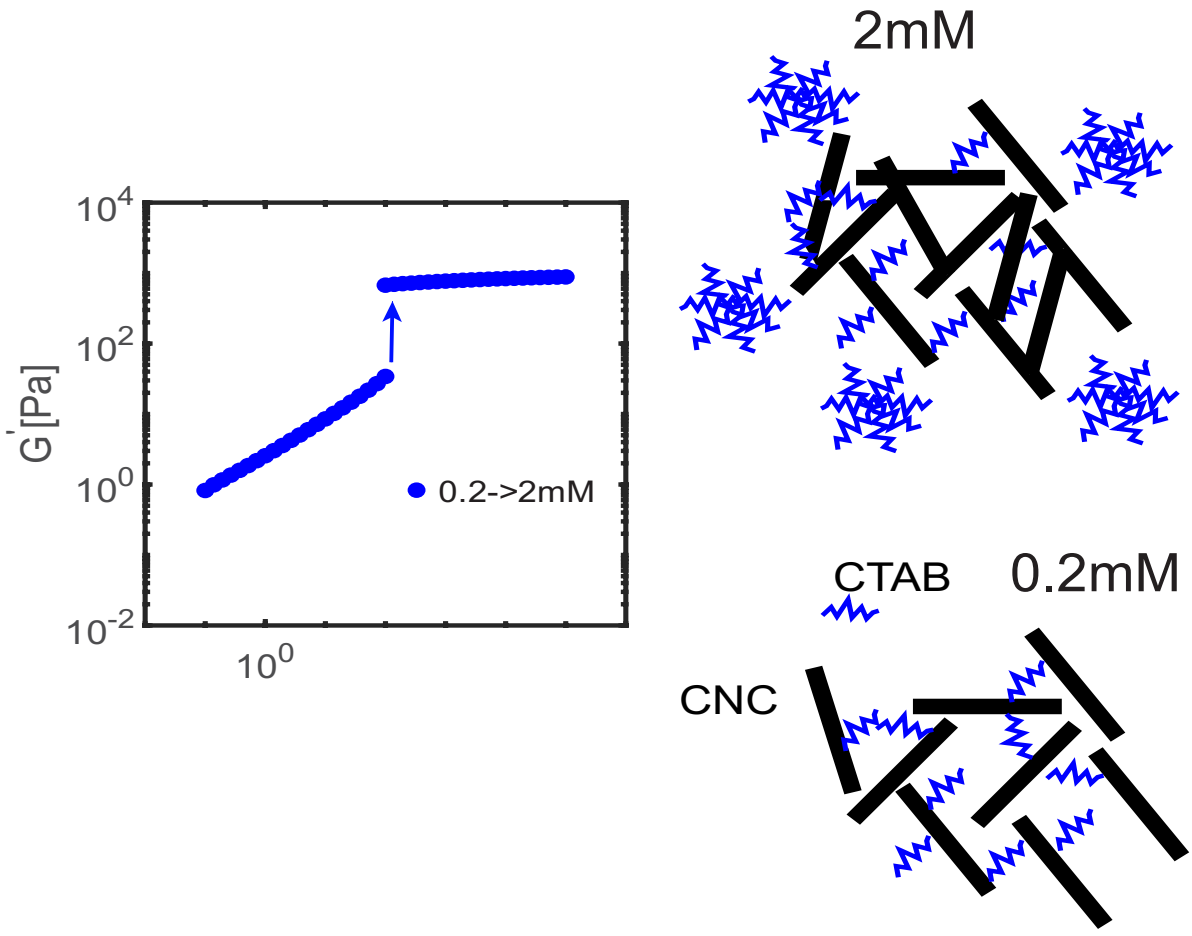

Preface

This research was conducted under supervision of Professor Savvas G. Hatzikiriakos in the Chemical and Biological engineering department at the University of British Columbia. I was responsible for conducting literature review, identifying the knowledge gap, constructing and evaluating hypotheses, defining objectives, designing experimental protocols, performing experiments, and compiling and interpreting the results.

Rheological experiments were condicted in the rheologu laboratories in conjunction with Professor Savvas G. Hatzikiriakos.

Table of Contents

List of Tables

List of Figures

Acknowledgements

First and foremost, I would like to thank God almighty for giving me the strength, knowledge, ability and opportunity to undertake this thesis and to persevere and complete it satisfactorily. Without his/her blessings, this achievement would not have been possible.

I take pride in acknowledging the insightful guidance and support of Professor Savvas Hatzikiriakos for his valuable time whenever I approached him to show me the way ahead. Nobody has been more important to me in the pursuit of this project than the members of my Family. I would like to thank my parents, whose love and guidance are with me in whatever I pursue. They are the ultimate role models. I would like to thank my amazing siblings Maryam, Mina, Pouya, Elmira, and my amazing nephew Bardiya for their infinite support and kindness. Additionally, I also want to appreciate Dr. Aref Abbasi Moud's and Marziyeh Danesh's efforts for my project. Last but not the least; I would like to thank all my friends for supporting me spiritually throughout my life.

Dedication

Dedicated to my wonderful parents, siblings, and nephew.

Chapter 1: Introduction

Cellulose is the most abundant organic compound on earth [1] which is the structural component of the primary cell wall of green plants, and can also be produced by a large variety of living organisms, such as algae, oomycetes, acetobacter, and rhizobium [2]. Biocompatibility, biodegradability, and thermal and chemical stability are properties of cellulose [1] which leads to the usage of cellulose in textiles fiber production[3], plastics[4], wood and paper products, coatings, cosmetics, and pharmaceuticals industries [5] . Raw biomass materials as the source of cellulose has introduced cellulose as the most abundant source or renewable energy [6].

Cellulose is a polysaccharide consisting of a linear chain of several hundred to over ten thousand β-D-(1-4)-linked glucose repeating units [6,7]. Also, numerous amount of intermolecular and intramolecular hydrogen binding in cellulose structure limits its solubility in water and typical organic solvents [6,8]. Such native intermolecular hydrogen binds cause the formation of microfibrils. These microphibrils have both crystalline and amorphous regions. The crystalline part of the cellulose have drawn interest for adapting them to miscellaneous applications [9].

Surface modification of cellulose to impart charges for suspension stabilization can be realised by various methods including hydrolysis[10], esterification [2,11], acetylation and acylation[2], cationization[2] , silylation[2], carbamination[2], TEMPO-mediated oxidation [11], and polymer grafting [11]. One of the most technologically important products from the above mentioned processes is cellulose nanocrystal (CNC). CNC possesses a number of unique properties such as biodegradability, renewability, nontoxicity, and sufficient mechanical properties, which leads to the usage of CNC in drug delivery[5] , tissue engineering[13], oil industry (oil-water separation[7], viscosity modification[8,9]) , adsorption of dyes[9] and pulp and paper [14] industries. Therefore, investigating and understanding the rheological properties (such as viscosity, linear viscoelastic behaviour, yield stress) and of CNC in the presence of surfactants and electrolytes would provide valuable information for the emergence of new applications and optimization of existing ones.

Hydrolysis of CNC leads to the formation of the sulfate group on its surface. The obtained CNC is able to form chiral nematic ordered structure above a critical concentration in the presence of

colloidal aqueous solution (deionized water)[13–15]. Above this critical concentration, formation of fingerprint texture can be observed[8]. However, sonication (Sonication affects the structure of suspensions by breaking agglomerations (by applying ultrasound energy) formed due to electrostatic and hydrophobic interactions as is the case for a common behaviour of lipotropic liquid crystal[16]) has a significant effect on these phases formed in these suspensions. The effect of sonication on CNC suspensions was investigated by Shafiei-Sabet et al[16] who have shown that by increasing the level of sonication in the range of 0 to 5000 J/g, the viscosity and other rheological properties of the samples significantly decrease. Beyond sonication, the addition of electrolytes and surfactants to CNC suspensions affect the rheological properties CNC suspensions significantly[9,17]. In particular, the effect of surfactants on hydrophilicity, stability and dispersion of CNCs in aqueous medium has been investigated, and the physicochemical properties of CNC suspensions have been characterized in the presence of different surfactants[10]. More recently Damoon and Hatzikiriakos [17] performed a systematic investigation of the effect of two oppositely charged surfactants with similar structure and carbon chain lengths (Cetyltrimethylammonium Bromide (CTAB), and Sodium Dodecyl Sulfate (SDS)) on the viscosity enhancement and gelation of CNC suspensions. Furthermore, they elucidated the possible mechanisms resulting in the adjustment of viscosity and gel formation by investigating the surface charge alterations of CNCs and the effect of ionic strength. They proved that by increasing the concentration of CTAB, the interconnected network develops and leads to gradual gelation of the chiral nematic CNC suspensions[17]. While SDS indicates both attractive and repulsive forces over different range of SDS concentration, it can be used to control the viscoelastic behaviour of CNC suspensions[17]. However, their study was performed for unsonicated samples, where large CNC agglomerations are present and thus gelation might be occurring easier in the presence of small number of surfactants.

The presence of electrolytes also affects the rheology of CNC suspensions and in fact they gelate CNC suspensions at certain concentrations. There are several studies on the subject of addition of NaCl or other electrolytes in the range of 10 to 15 mM to the isotropic CNC suspensions (3 wt%). They result in extensive aggregation, as well as higher viscosity and shear modulus[13]. In another study[18] the effect of 20 mM NaCl and $CaCl_2$ on the rheological behavior of both CNCs and electrostatically stabilized crystalline nanocelluloses (ECNCs) demonstrated that ECNCs could

withstand much higher ionic strengths than CNC suspensions. They form gels even at really low concentrations due to agglomeration. More recently Danesh et al[19], investigated the effect of electrolytes on the rheology of CNC suspensions using extremely high NaCl concentration up to 50mM. They identified that these systems possess two yield stresses. The first yield stress at low shear rates is attributed to the disconnected CNC clusters as a result of bond breakage. The second yield point occurs at higher shear rates and it is related to the deformation of clusters, where individual nanorods are completely separated and dispersed. It perhaps becomes important to combine a small amount of an electrolyte with a small amount of a surfactant to identify possible synergistic effects.

Chapter 2: Literature Review

2.1. Chemical Structure of CNC

Chemical structure of CNC play a crucial role in its vast functionality as CNC is a polymer consists of six hydroxyl groups within the repeating structure of β-D-glucopyranose units[20]. Additionally, its structure provides high surface area which increases its tendency to bond with other components. It is considered as an reinforcement of transparent resins because of its nano size fibres (at least one dimension equal or less than 100 nm [21]), high specific surface area[21], and being less than one-tenth of the visible light wavelength[22].

2.2. Extraction and Preparation of CNC

There are two ways to produce nanocellulose: top down and bottom up. Top down method which reduces the size of the fibres mechanically leads to the production of cellulose nanofibers (CNF) as well as CNC [23]. The bottom up approach (implies understanding the building blocks and then assembling them into a useful structure[24]) has been used to obtain bacterial cellulose (BC) methods generate nanoparticles by building them from drug molecules in solution.

There are various sources that can be used to extract cellulose and processing on the obtained material leads to the production of the CNC. One of the processing methods which has been used in this research is acid hydrolysis (isolating cellulose with acids such as hydrochloride acid, sulfuric acid, phosphoric acid and bromic acid. During the hydrolysis as the amorphous region has weak resistance to acid, it will dissolve but the crystalline part will remain intact).

In acid hydrolysis the choice of acid is an important factor as it affects the properties of the obtained nanocrystals. There are two types of the acids that can be used for this process which are sulfuric acid and phosphoric acid. Both acids introduce negative charge on the nanocrystal (sulfate or phosphate group) and leads to the electrostatically stabilization of the nanocrystal suspension. Considering that sulfuric acid induces much higher surface charge density on the nanocrystal, in this research this method has been considered[15].

2.3. Rheology Properties of CNC

Shafei- Sabet et al. investigate the rheology properties of a synthesized CNC by acid hydrolysis of black spruce kraft pulp using 64% w/w sulfuric acid at 45 °C for 25 min, according to Hamad and Hu protocol [14] in their laboratory. Zeta potential (electrokinetic potential) has shown the effect of sonication on the physicochemical properties (such as conductivity, particle size, charge distribution, and microstructure which give us a broad understanding of the chemical structure od CNC's aggregations) and particle dimensions of CNC by analysing the forces on the solid or liquid which are happen either as a change in the charge or electrostatic potential of the suspensions[25]. In their investigation they have shown no changes in the dimensions of the individual nanorods by increasing the level of sonication more than 2000 J/g. The size change observed from zetasizer measurements can be attributed to breakage of aggregates, but not the individual rods themselves[16] Also, the energy supplied at levels less than 500 J/g was insufficient to break the covalent sulfate ester-cellulose bonds at room temperature [16]. As sonication has a significant effect on these phases formed in these suspensions, they have shown that by increasing the level of sonication in the range of 0 to 5000 J/g, the viscosity and other rheological properties of the samples significantly decrease. Sonication affects the structure of suspensions by breaking agglomerations formed due to various forces (ultrasound energy in a medium, leads to the formation of energy density gradient in the direction of propagation which is as a result of energy absorption from the acoustic beam[26]. Additionally, in liquid this energy gradient is correlated with the generation of acoustic streaming due to the transfer of momentum to the fluid and is also connected to the radiation pressure phenomenon[26]) as is the case for a common behaviour of lipotropic liquid crystal. The viscosity profiles of well sonicated samples show two shear thinning behaviour at low and high shear rates and a plateau in between as a result of various structures developed. Also, their isothermal frequency sweep tests illustrate that over a critical concentration on CNC, the storage modulus (G′, which is related to the energy that has been stored in a material) is nearly independent of the frequency and surprisingly higher than loss modulus (G″, which is related to the energy that has been dissipate by making deformations) which implies the formation of gel-like materials.

Shafei-Sabet et al. also investigated the effect of degree of sulfation on the rheology of CNC[27]. The synthesized particles named CNC-A and CNC-B, based on the Hamad and Hu protocols [14,27]. CNC-A had sulfur content of 0.85 wt%, while CNC-B had 0.69wt%. In addition, the acid/pulp ratio in ml/g for CNC-A and CNC-B were 8.75 and 6.00 in order. The effect of sonication coordinated in a similar fashion as their previous work on CNC[16] (after 1000 J/g the breakage in the aggregates is obvious) in order to make a comparison; therefore, they prepared 1-15 wt% of the both CNC and they applied 1000 J/g level of sonication on them in order to study their viscosity behaviour by steady shear test. It has been shown that for the CNC-A with higher concentration of sulfuric acid the viscosity curve experiences behaviour like isotropic samples. Increasing the concentration over 3 wt% leads to the formation of liquid crystal phases following three-region profile in viscosity that is a typical behaviour of the liquid crystals[27]. By increasing the CNC concentration from 7 to 15 wt% the viscosity profiles experience a change to a single shear thinning behaviour over the whole range of shear rates. This indicates a transition from liquid crystal to gel like structure. CNC-B with lower concentration of sulfuric acid experienced the same behaviour but at various concentrations. It exhibited behaviours like isotropic samples below 4 wt% of CNC, and then gel like behaviour at concentration over 10 wt%.

Polarized optical microscopy (POM) has shown that the CNC-A had fingerprint structure at 3 wt%, the fraction of liquid crystal domains in biphasic system increases at 7 wt%, the CNC suspension with 9 wt % has shown cholesteric liquid crystal morphology, and finally above 12 wt% birefringent gels has been obtained with no fingerprint. CNC-B POM test has shown no liquid crystal phases at 3 wt%, the fingerprint patent has been shown at 5 wt%, and the fingerprint gels appeared at 10 wt%.

The linear viscoelastic behaviour of the CNC-A showed different behaviours at different concentrations which are liquid like, gel like, and solid like at 10 wt% and lower, 12 wt% and 15 wt% of CNC concentration respectively. While the same behaviour appeared for CNC-B, however at different concentration mainly due to surface charge differences[27].

Damoon and Hatzikiriakos investigated the effect of CTAB from (0.2-6 mM) on the rheology of 3 wt% CNC suspensions. The 3 wt% CNC suspension behaves like a viscoelastic liquid over the whole range of angular frequency with G″ to be greater than G′. Addition of CTAB results in

electrostatic interaction between the hydrophilic head of the CTAB and the negative charge of CNC rods. Addition of 0.2 mM CTAB to CNC suspension has shown weak entanglement within the CNC rods with G´to be greater than G″ at high frequencies and G″ to be greater than G´at lower frequencies. The addition of CTAB over 0.4 mM showed gel like behaviour and stronger bonds between CTAB and CNC as G´ was greater than G″ over the entire frequency range; therefore, 0.4 mM CTAB considered as the concentration in which suspension commenced exhibits crosslinks between CNCs. By further increasing the concentration of CTAB from 0.6 to 0.8 mM, formation of admicelles on the surface of the CNCs have been hypothesized. Meanwhile, the addition of CTAB over 0.8 mM resulted in aggregation. In order to confirm their rheological findings, they studied the effect of ionic strength of surfactant on the rheology of CNC in the presence of CTAB and NaCl in association with zeta potential measurements.

Addition of NaCl to CNC leads to the decrease in G´ which is explained by the compression of double layers (by increasing the concentration of the NaCl, first the electrostatic force is dominant which leads to the screening of the charge, afterward the hydrophobic forces lead to the formation of the double layer) around the CNC rods. Hence, not only the aforesaid compression decreases the interactions between CNCs, but also the particle size decreases as a result of the repelling forces. Such trends minimize the attractive forces between adjacent CNCs as well.

Meanwhile, increasing the concentration of NaCl over 1 mM leads to the formation of hydrogen bonds and van der Waals forces. Therefore, increase in attractive forces leads to the formation of the interconnected network within CNC suspension. Therefore G´ experienced greater value than G″. At 6 mM of NaCl a viscoelastic solid like behaviour appeared, which results into a transition from a viscoelastic liquid (at 4 mM) to gel transition. Although the addition of 8 mM NaCl provided stiffer solid like suspension, while above 8 mM no change has been observed which indicates that the suspension has reached its equilibrium state.

Their zeta potential investigation agreed with their rheological findings as it showed a decrease in ionic strength for CNC/ NaCl suspension with mild slope with an increase between 4 mM to 6 mM NaCl (attractive forces overcome the repulsive behaviour). Subsequently, CNC/CTAB suspensions followed the same trend as CNC/NaCl suspensions.

Sahlin et al. compared properties of unmodified CNC and modified CNC with salts onto the sulfate ester groups on the cellulosic surface[28]. They have shown that the shear viscosity and G' and G" have been increased remarkably as a result of the attraction interactions between grafted substitutes[28]. They also concluded that a more hydrophobic character of the CNC surfaces could be beneficial, when using CNC as reinforcing elements in a polymer matrix composite[28].

As discussed above, well-sonicated samples of CNC display three distinct rheological zones, namely, two shear thinning behaviours at low and high shear rates and a plateau at intermediate shear rates, as a result of the development of liquid crystal formation and ordering[18]. Increase in CNC number density (here is probed as concentration), to reduce excluded volume, the particles self-assemble into chiral nematic ordered structures that display fingerprint texture[18,29,30]. Sonication impacts the structure and rheology of CNCs, through demolishing of the initial clusters formed during air drying pre-processing of CNC[16,18]. Breaking of agglomerates leads to (i) overall higher aspect ratio of CNC colloidal system (ii) higher localized dense liquid crystalline regions and lower effective volume fraction of CNCs that significantly reduces the viscosity[12].

In the presence of electrolytes, the rheology of CNC suspension dramatically changes, i.e. higher viscosity, appearance of yield stress and high shear modulus, due to network formation and coagulation[31–34]. In particular, recently Danesh et al.[19], through alteration of level of added salt affected the attraction strength of CNC colloidal systems and found appearance of two yield stress points at low and high shear rates, attributed to the disconnection of link between CNC clusters through bond breakage (first yield stress) and the deformation of clusters, where individual nanorods are completely separated and dispersed (2^{nd} yield stress). The rheological behaviour of CNC suspensions in the presence of surfactants was found to be similar, however, the gelation mechanism changes below and above CMC[17].

The yielding process, a complex phenomenon but highly applicable to industrial applications has been the subject of many studies in the literature[35]. For instance, start-up of steady shear flow experiments on attractive glasses[36] and colloidal gels[36–38], show two yielding process, through the appearance of two unique stress maxima. Oscillatory shear flow and step strain experiments also show two yielding step process[39,40]. The first maximum is due to bond breaking; however, the

second maximum is related to cage breaking in colloidal glasses and cluster breaking in colloidal gels[41]. At lower volume fractions, gels do no show the two yielding step transition[42]. These two yielding steps has been seen in a variety of complex systems[43–46]. For CNC gels, yield stress has been studied recently in the literature[47]; however, the understanding of the yielding in CNC hydrogels still remains poor.

Chapter 3: Thesis Objectives and Organizations

As the rheological behaviour of the CNC-CTAB gel, in suspension and gel form, has industrial and academic importance, it is investigated in detail in the present study. Previously the CNC-surfactant gelation has been explored by Ranjbar and Hatzikiriakos[17] and Kushan et al.[48], however many aspects of the rheological behaviour of CNC-CTAB still remain unknown. The system studied in the present work is an attractive gel[49] that display tuneable range of attractions and attraction strength due to charge screening of CTAB micelles (negatively charges) and CTAB molecule (positively charged head) length that is ~ 4nm. The system under study is viewed and studied from the colloidal perspective. In detail, in the present work we explore the linear viscoelastic behaviour, the effect of sonication on rheology of the CNC-CTAB system, its thixotropic, and yielding behaviour as a function of CTAB content and level of sonication below and above the critical micelle concentration (CMC).

Chapter 4 presents the materials used in the present work, the method and details of their preparation and the experimental methods for their analysis. Chapter 5 presents the main results of this work. As discussed above presents a nearly complete rheological study of the CNC suspensions (sonicated) in the presence of a positively charges surfactant. Finally, Chapter 6 presents the main conclusions from this work.

Chapter 4: Experiments

4.1 Materials

CNCs were purchased in spry dried from CelluForce Inc. (Montreal, Québec, Canada) with a sulfur content of 0.89wt%, as reported by the supplier. CTAB with reported 98% purity was purchased from Sigma-Aldrich. For making the surfactant solutions and CNC suspensions, deionized (DI) water was used. According to the manufacturer, CNCs nominal length, and diameter are 150 nm, and 7.5 nm, respectively, and therefore have an aspect ratio of about 20^[45].

According to Solomon[50] and Spicer, there exist three concentration regimes in suspensions, in the non-interacting limit, i.e. $\varphi \ll 1/(L/b)^2$, $1/(L/b)^2 \ll \varphi \ll 1/(L/b)$ and $1/(L/b) \ll \varphi$ that corresponds to dilute, semi-dilute and concentrated regimes, respectively, where φ is the volume concentration of the CNC suspension, L is the fiber length and b is the fiber diameter. Assuming CNC density equal to 1600 kg/m^3, the CNC volume fraction for the 5wt% samples mostly used in the present work is estimated as 3.2vol%. Therefore, considering the aspect ratio of about 20, the prepared samples are in the semi-dilute regime. In this concentration regime, each CNC has a few direct contacts with its neighbours. However, Brownian dynamics of the suspension is a strong function of the number density of floating particles influenced also by the electrostatic forces of the negatively charges fibers giving rise to a plurality of rheological behaviour. Particle rotations are hindered as the mean separation distance between CNC is less than the individual CNC fiber length (150nm).

4.2 Materials Preparation

CNC suspensions with 5wt% concentration was prepared by dissolving 5g CNC powder in 95ml DI water in beakers. Suspensions were stirred for 4 h to obtain homogenous suspensions. Surfactant stock solutions of 5wt% were prepared to produce suspensions of CNC-surfactant of various concentrations. To prepare a stock solution of CTAB, 5g of CTAB powder was added progressively to a 100mL beaker containing 95g of DI water, while being stirred on a hotplate

immersed in a 50°C bath. The stirring continued for roughly 30 min until the CTAB powder was fully dissolved and the solution stabilized.

Having the surfactant stock solutions, CNC samples with surfactants were prepared by introducing 20mL of CNC suspension into a 100mL beaker. Appropriate amounts of surfactant solutions (ranging from 0.0219 to 1.1793mL for CTAB) were added to the beaker, while being stirred at 500rpm, to obtain the desired surfactant concentrations (0.2 to 2mM for CTAB). The stirring continued for 2h followed by 1min of centrifugation at 1000rpm to remove bubbles. The samples were stored for 12h before any further characterization to ascertain that the samples have adequately recovered from any disturbances in their microstructure resulting from the shear applied to the suspensions. Additionally, since factors such as temperature, pH of the solution, and ionic strength of solution have a significant impact on surfactant adsorption, they were kept constant for all samples studied[51].

After the preparation of samples, sonication was applied on a 5wt% CNC suspension sample at the input energy level of 500J/g. The sonication level was chosen to obtain a similar viscosity profile of the 3wt% of unsonicated CNC suspension reported by Ranjbar and Hatzikiriakos[17] with that of 5wt% of sonicated samples in this study. One of the objectives of the current study is to identify the effect of sonication on the performance of surfactants as rheology modifiers (gelation). Sonication levels up to 5000 J/g were also applied to selected CNC-CTAB suspensions/gels to study the full effect of sonication on the rheological behaviour of these suspensions.

4.3. Materials characterization

4.3.1 Zeta potential

The zeta potential of CNC particles (prior and after the addition of surfactants) was measured employing disposable plain folded capillary zeta cells (Malvern Zetasizer Nano ZS). The zeta potential was calculated from the electrophoretic mobility using the Helmholtz–Smoluchowski equation at 25 ^{O}C. The concentration of CNC suspensions was 0.25 wt% in water with up to 2 mM CTAB. All zeta potential data points were the average values of 3 measurements

with 20 cycles per measurement. Zeta potential is measured by the formula blow where $\boldsymbol{dl_{str}}$ is the slope of streaming current, $d\Delta p$ is differential pressure, ε is dielectric coefficient of surfactant, ε_0 is permittivity, L is length of the streaming channel, and A is cross section of the streaming channel.

$$\zeta = \frac{dl_{str}}{d\Delta p} \times \frac{\eta}{\varepsilon \times \varepsilon_0} \times \frac{L}{A}$$

4.3.2 Rheology

Rheological characterizations were carried out using the MCR 502 (Anton Paar) rotational rheometer equipped with parallel-plate geometry (50mm in diameter and gap size of 0.5mm) at 25˚C. A thin layer of mineral oil was applied to the periphery of the sample to avoid sample evaporation during the experiment. To get consistent results the following protocol was used for all rheological measurements. Before any rheological testing, and after loading the sample, a pre-shear of 400 1/s for 1min (shearing time) followed by 30min rest (recovery time) was applied (constant shear rate from 200-700 1/s applied on sample to determine the optimised value for pre-shear) . The initial pre-shearing breaks all the flocs into nearly individual rods. The complex viscosity after this initial pre-shearing reaches a certain level (using a time sweep at a small frequency of 1 rad/s and strain amplitude of 1%), which implies that the suspension is in a nearly fully disassociated state. A 30-min rest time was considered after pre-shearing to allow the suspension to rebuild its structure. Rest times longer than 30 min did not increase the complex viscosity and/or modulus further (using a time sweep at a small frequency of 1 rad/s and strain amplitude of 1%), which was used as a way of checking the full recovery of the structure of the CNC suspension.

Steady-shear was performed over the range of shear rates ($\dot{\gamma}$) from 0.01 to 100s^{-1} to obtain the viscosity of pure CNC suspensions and those with various amounts of surfactants. These tests were performed in two ways, from low-to high shear rate (labelled as L-H) and from high-to low shear rate (labelled H-L) by allowing enough time for each shear rate to reach steady-state monitored by the shear stress level. Amplitude sweep experiments were performed at a frequency of 1rad/s to determine the range of strains over which the samples exhibit linear viscoelastic (LVE) behaviour.

These experiments provide useful information for the yielding behaviour of the various suspensions as well. Creep testing on selected samples were performed to verify the yield stresses obtained from amplitude sweep and steady-shear experiments. Frequency sweep tests were performed over angular frequencies in the range from 0.1 to 100rad/s to determine the linear viscoelastic moduli (loss and storage modulus) of pure CNC and surfactant-loaded CNC suspensions.

$$\gamma(t) = \gamma o \sin(\omega t)$$

$$\sigma(t) = \gamma[G'(\omega)\sin(\omega t) + G''(\omega)\cos(\omega t)]$$

Chapter 5: Results and Discussion

5.1 Effect of CTAB concentration on zeta potential

Figure 1 displays the zeta potential of suspension of CNC with concentration of 0.25wt% as a function of CTAB concentration. After increasing CTAB concentration to 0.2mM, zeta potential decreases in absolute value from ~-55mV to -35mV due to screening the negative charges of CNC by positive end groups of CTAB. This development sets the stage for colloidal instability and gel formation in suspension of CNCs. Based on **Figure 1**, the trend in decreasing the zeta potential is incremental and steady as opposed to that in the case of electrolytes such as NaCl reported in the literature[17,52]. It is also interesting to note that around 1mM (point of micelle formation), charge reversal occurs from negative to positive due to formation of micelles. Initially, zeta potential trend from negative to zero can be ascribed to formation of hemimicelles, that is, surfactant monolayers, at the expense of electrostatic adhesion between head part of CTAB and CNC with negative charge. Then, once the concentration reaches to 0.05-25mM, mixed hemimicelle forms through hydrophobic and electrostatic interactions between tails of CTAB molecules. Ultimately, at higher CTAB concentrations, hydrophobic interaction leads to formation of CTAB bilayers[33,53]. Therefore, at this stage, surface charge of admicelles becomes positive and leads to positive reading of zeta potential[13]. The results of this section explain the rheological changes with CTAB concentration that are discussed in subsequent sections.

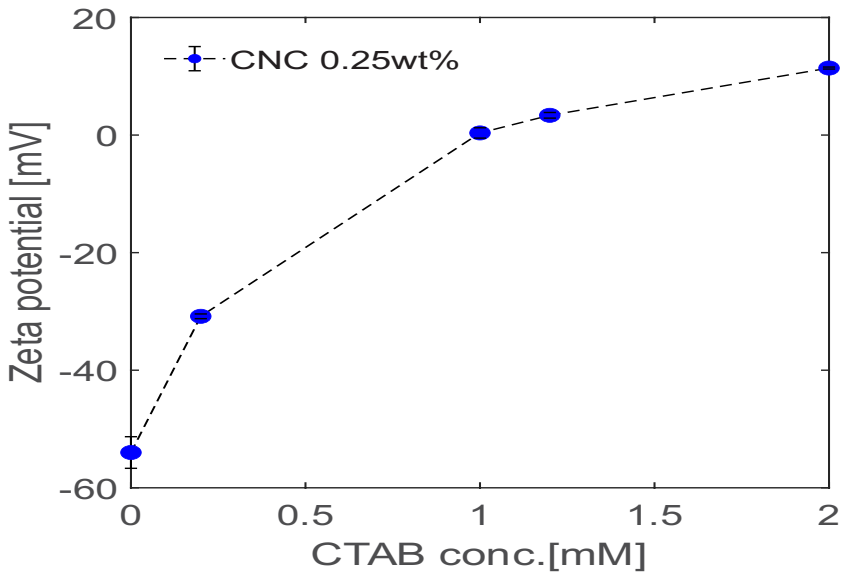

Figure 1. Zeta potential versus the concentration of CTAB for 0.25 wt % CNC suspension. The parallel lines represent error bars associated with each data point; moreover, dashed line has been sketched to guide the eye along the direction of changes in zeta potential.

5.2 Effect of pre-shear

The typical rheological experiment is composed of placing the sample in a reproducible initial state, by applying a certain protocol and subsequently letting the sample to recover autonomously its structure for a period of pre-defined rest time as discussed above. This is necessary to generate reproducible results and diminish the effect of shear history on rheological measurements. As discussed in section 2.1, samples were pre-sheared at 400 s^{-1} for 1 min and were left to rest for duration of 30 mins to recover a quasi-similar micro-structure. Within this period, through monitoring complex modulus and viscosity at small shear strain amplitude of 1% and at low level of frequencies (1 rad/s), it was observed that system reaches to a nearly steady state condition after approximately of 30 minutes (**Figure 2**). It appears that resting time of 30mins is enough to let thermal motions reorient CNCs in vicinity of one another for reaggregation as previously has been mentioned by many [54–56].

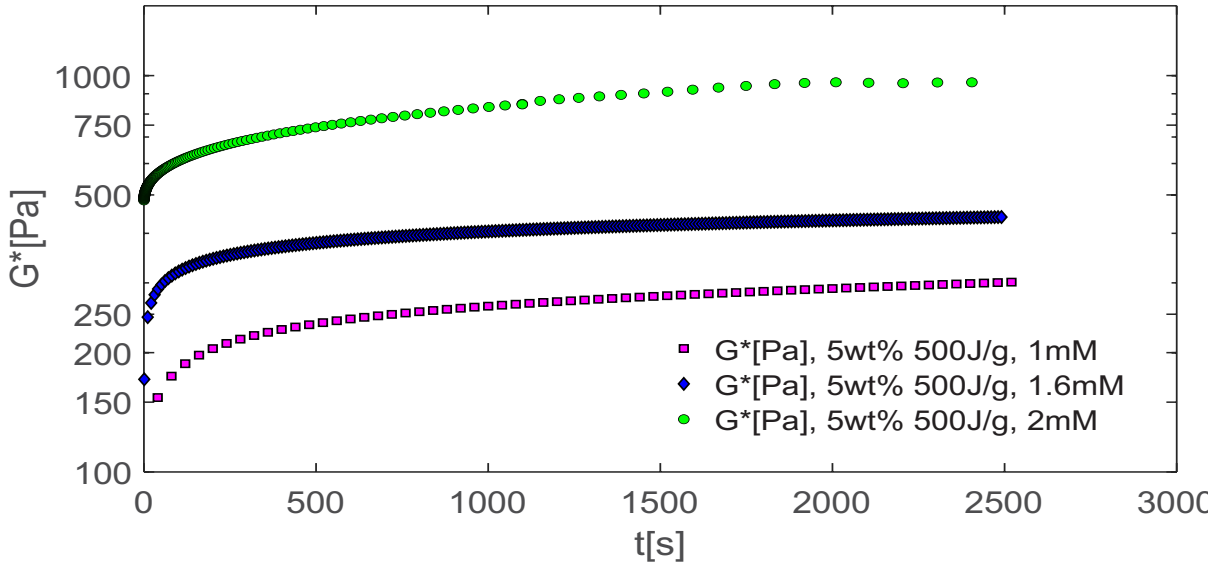

Figure2 . Structure recovery after pre-shear: complex modulus, G* (ω) versus time using a strain amplitude of 1% and a frequency of 1 rad/s for samples containing 1mM, 1.6mM and 2mM CTAB.

5.3 Effect of sonication and concentration on CNC suspension

To probe the impact of ultrasound energy input on the rheological behaviour of CNC suspension, energy input ranging between 0 to 500J/g was applied to various loadings of CNC and their steady-state shear viscosity was compared with results from Rajbar and Hatzikiriakos[17]. As noted above one objective of this work was to compare the effect of surfactants on the rheological behaviour of CNC suspensions with and without sonication at similar viscosity levels. Therefore, we were investigating to obtain a viscosity match between 3wt% unsonicated[17] CNC suspension with 5wt% sonicated to a certain level which is determined below. **Figure 3a** shows the shear-thinning behaviour for the suspensions of CNC 5wt% at different levels of sonication. The unsonicated sample (3wt% CNC) shows a single shear-thinning regime, however, as the level of sonication increases, the complex viscosity drops nearly two orders of magnitude at the sonication input energy of 500J/g due to gradual breakup of agglomerates. At this level of sonication, the viscosity profile shows first a tendency for a Newtonian plateau at low shear rates followed by a shear thinning behaviour at higher shear rates, a tendency for a second plateau at high shear rates (not seen here), typical of an isotropic sample. For higher shear rates a second shear-thinning regime appears. These regimes have been shown more clearly at higher sonication levels[16]. The appearance of a second plateau at intermediate shear rates implies liquid crystalline behaviour of

CNC suspensions, which stems from the formation of chiral nematic phases (seen in **Figure 3a**) for the highest level of sonication of 500J/g. At low shear rates, the alignment of chiral nematic domains in the shearing direction results in a shear-thinning profile followed by a plateau at intermediate shear rates with all domains oriented along the shearing direction[17,57] At high shear rates, the liquid crystal domains are destroyed by the applied stresses making it possible for every single nanorod to align in the shearing direction. Inspecting the viscosity profiles, it can be concluded that there is still room for breaking up of the agglomerates by sonicating the samples beyond 500J/g. The size of primary particles can still scale down to lower values thus decreasing further the viscosity profile and the viscoelastic moduli of the suspensions (shown below).

As it is visible in **Figure 3a**, there is a match between the viscosity profile of 5wt% sonicated at 500J/g with the unsonicated 3wt% suspension (**Figure 3a**). Therefore, experiments in this work will be performed for 5wt% CNC sonicated at 500J/g[17] and the results will be compared with those reported in for 3wt% CNC unsonicated. This comparison will address the confounding effect of sonication (mainly particle size) and surfactants on rheological properties. To further consolidate our hypothesis that microstructurally 3wt% CNC unsonicated sample and 5wt% CNC sonicated are almost the same, strain sweeps of the two samples were measured and depicted in **Figure 3b**. As can be seen, the viscoelastic moduli match well particularly at low strains where linear viscoelasticity prevails. However, there is a mismatch between non-linear rheological behaviour of the two samples at higher strain amplitudes, as expected, due to the dynamics of floc breakup at higher shear strain amplitudes.

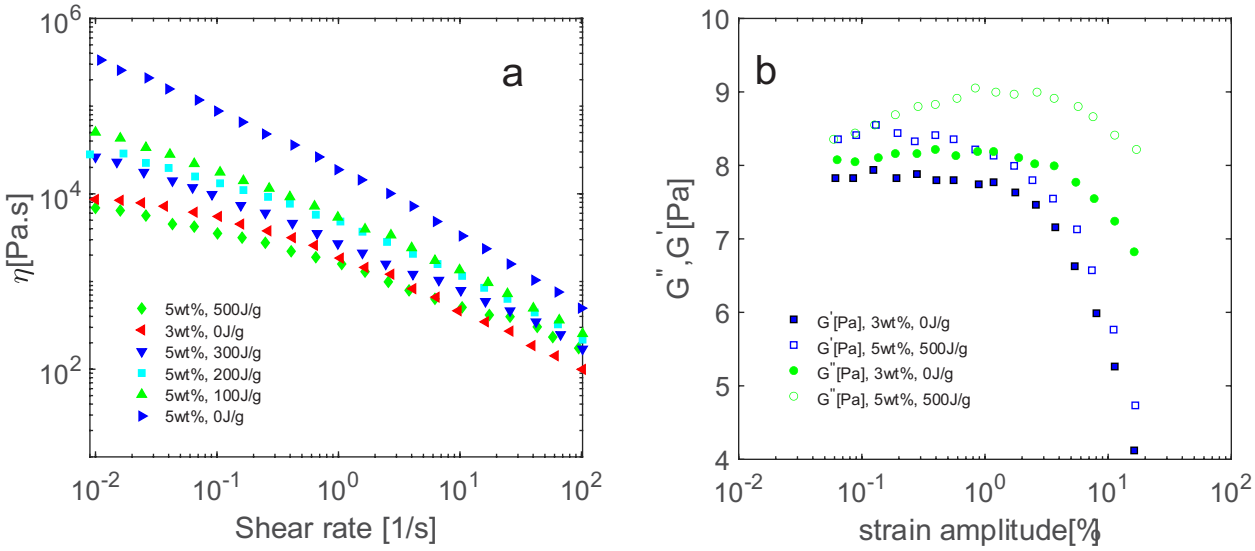

Figure 3. a Steady-state shear viscosity (η), versus shear rate ($\dot{\gamma}$) for CNC suspensions 5wt% at various levels of sonication and 3wt% unsonicated at 25°C sketched on double logarithmic scale. b Storage modulus and loss modulus versus shear strain of unsonicate 3wt% CNC, and 5wt% CNC sonicated at 500J/g sketched on semilogarithmic scale.

5.4 Effect of CTAB incorporation on viscosity profile

Figure 4a shows the effect of CTAB on the shear viscosity of 5 wt% CNC suspensions in the presence of various amounts of surfactant (0-1.8 mM). The measurements in **Figure 4a** were performed from low-to-high shear rate labelled as L-H while those in **Figure 4b** from high-to-low shear rate labelled as H-L. Upon addition of CTAB, surfactant molecules are attracted to the surface of CNCs from their hydrophilic head, due to the electrostatic attractions between the positive head of CTAB and negative sites (sulfate ester groups) of CNCs. The attraction of CTAB molecules to the surface of CNCs, due to screening of the charges, diminishes the repulsion forces between nanoparticles and causes retraction of double-layer around CNCs[17,58]. Moreover, the hydrophobic attraction between the tails of CTAB molecules contributes to attraction forces between two individual CNCs. As a result, the CNC particles start to aggregate due to weak attraction forces and the viscosity at low shear rates increases by more than 3 orders of magnitude. It also noteworthy that there is a jump in viscosity values at CTAB concentration of ~ 1mM, i.e. the point of CMC (discussed in detail below). In comparison to individual surfactant molecules, CTAB in micelle form is compact and can act as a stronger coagulant as Kushan et al[48] also pointed out the same conclusion. Moreover, comparing the effectiveness of surfactant and simple electrolyte ions (NaCl) in affecting structure of CNC gels, in Ranjbar and Hatzikiriakos[17], a

comparison of zeta potential of CTAB-CNC and NaCl-CNC system revealed that approximately an order of magnitude lower number of positive ions has to be added to the system to cause a similar decrease in the absolute value of zeta potential. This observation reveals the different arrangements of CTAB molecules in the diffuse layer of double layer as opposed to sodium ions. It seems that an incremental increase in stress is required to initiate flow at various CTAB levels (see **Figure 4c and 4d**). The structure does not saturate even at vicinity of 2mM CTAB concentration, perhaps due to incomplete coverage of all CNCs by the surfactant molecules. In the ref[17], saturation happens at around 2mM of CTAB concentration for 3wt% unsonicated samples and further addition of CTAB does not cause an increase in the stress levels of the flow curves. The addition of more CTAB surfactant molecules leads to the formation of freely floating micelles in the suspension that does not contribute to the CNC-CNC network in the case of unsonicated samples. This interesting observation will be clarified and discussed later, once we compare the stress values required for flow as a function of sonication and CTAB content.

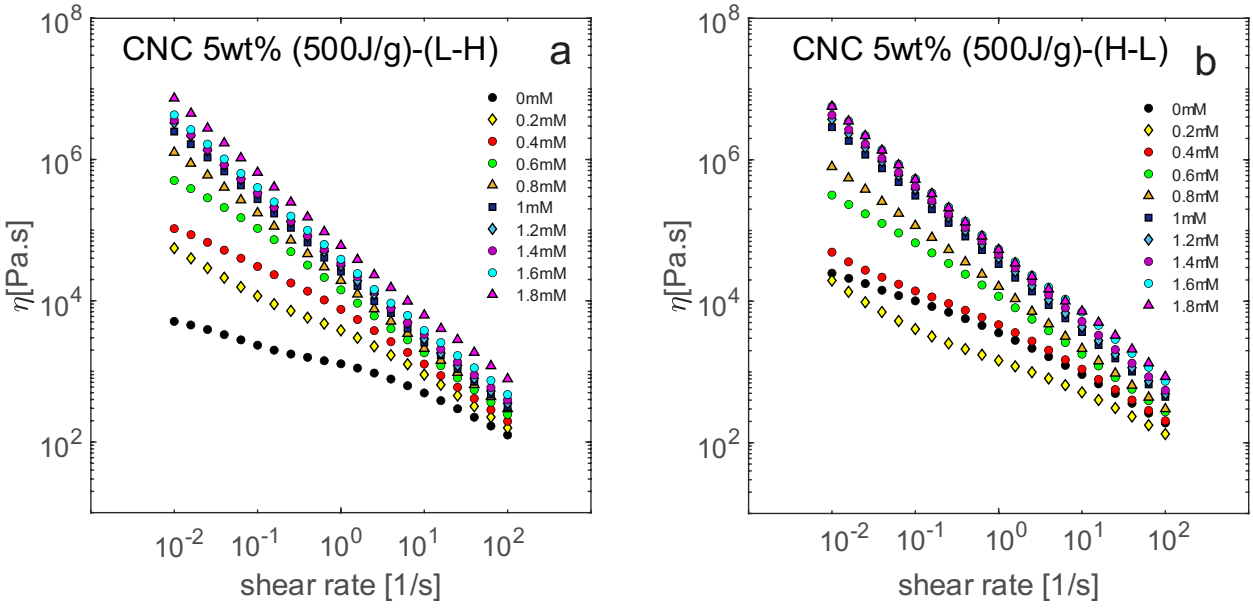

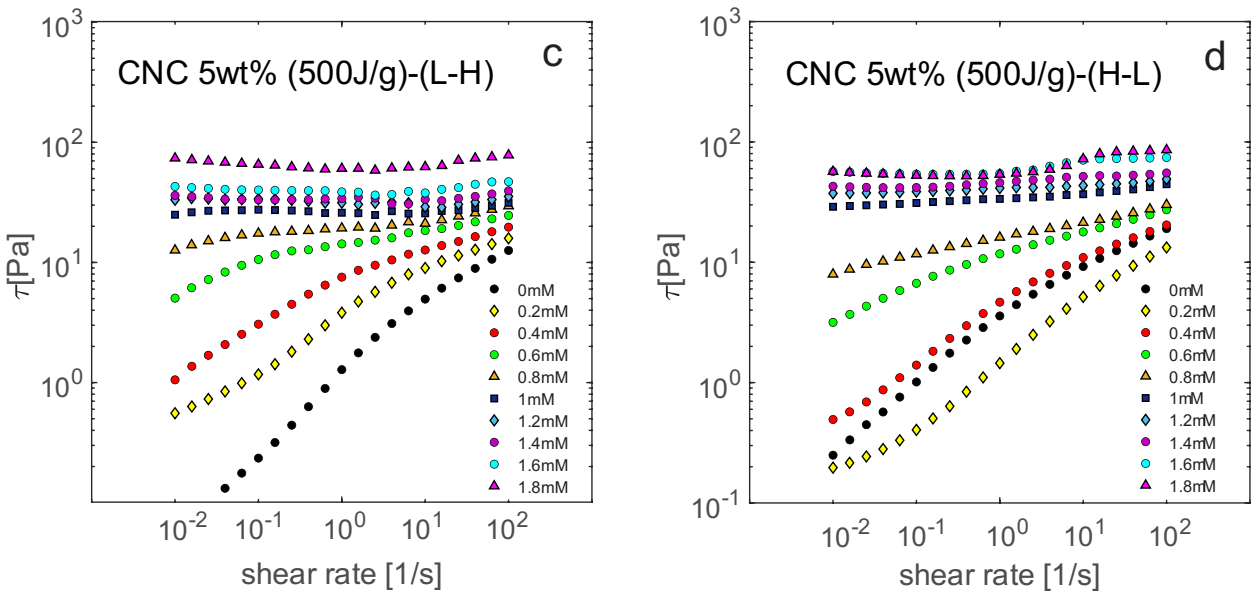

Figure 4. The shear viscosity and shear stress of CNC-CTAB gel/suspension with CTAB concentration of 0-1.8mM as functions of shear rate (a: viscosity using the low-to-high shear mode, b: viscosity using the H-L shear mode, c: shear stress using the L-H shear mod e and **d**: shear stress using the H-L). The shear ramp has been applied from 0.01 to 100 (labelled as L-H) and then reversed (labelled as H-L) after shearing the samples at a shear rate of 400(1/s) for a period of 60 seconds.

Overall, considering the interactions between CNC particles and surfactant molecules in this regime, aggregation is driven mainly by hydrophobic effects, minimization of surfactant tail-water interfacial area through migration of the tail of the surfactant unimer from bulk water to the assembly core with the simultaneous release of water of hydration, and an increase in the entropy of the system. Equilibrium is achieved through the combination of electrostatic, ion-specific, and hydration type interactions in the interfacial area between clusters of CNCs. Comparison between **Figure 4a (L-H)** and **Figure 4b (H-L)** shows there is a difference between shear viscosity due to different shear history, therefore, assessment of thixotropic behaviour of CNC-surfactant gel will be the focus of the next section (**section 3.4**).

Figure 4c and **4d** show the corresponding shear stress. Overall, all samples show shear thinning behaviour after overcoming a yield stress unique to each CNC-CTAB hydrogel sample. At high CTAB concentration the evidence of plateau at lower shear rates implies the existence of yield stress which increases with increase of CTAB concentration. More details and discussion on yield stress is presented in **section 3.6**.

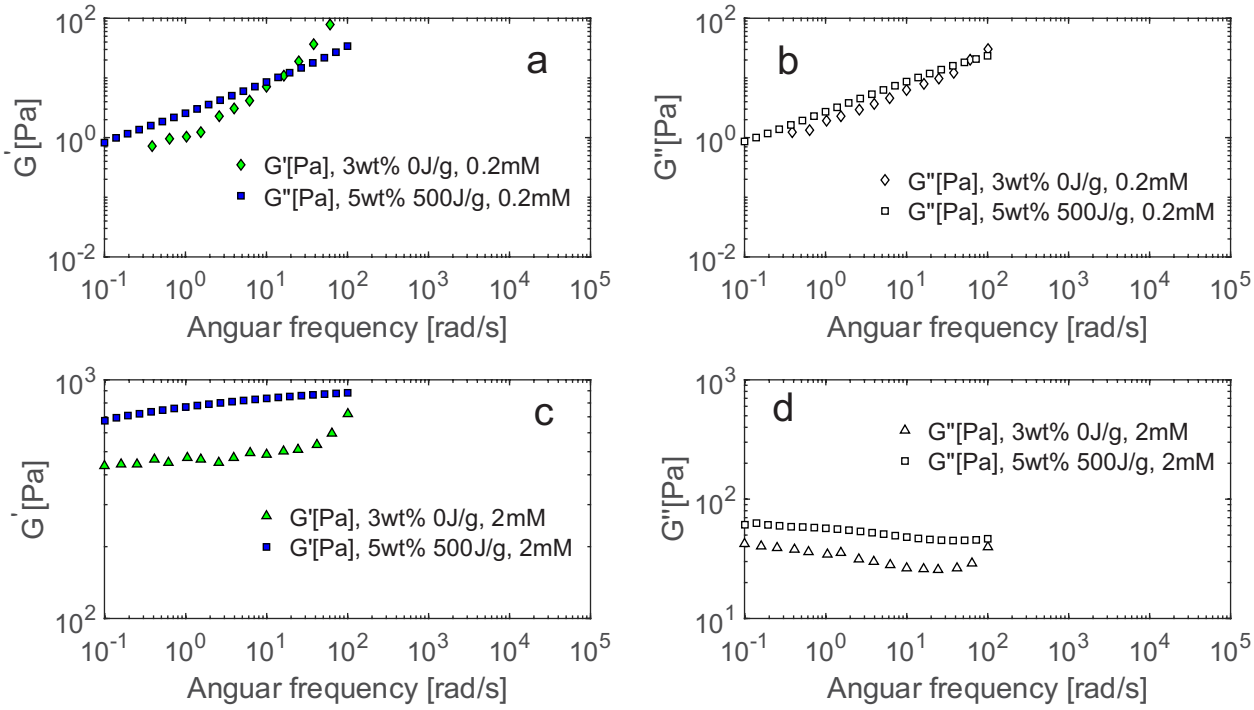

Figure 5. Linear viscoelastic characterization of CNC-CTAB solutions/gels for 3wt% and 5wt% CNC concentration and at different CTAB concentrations and sonication energy. Storage modulus (G') and Loss modulus (G''), of CNC/CTAB solution has been sketched on double logarithmic scale at different CTAB concentrations for strain amplitudes of 1% using a parallel plate geometry (50 mm in diameter, and gap size of 0.5 mm) at 25˚C. Results of unsonicated samples reported in paper[17] has been sketched with solid symbols.

Figure 5 compares the results of current paper (5wt% CNC sonicated at 500J/g) with those in our previous work[17] (3wt% unsonicated) to address the relative importance of CTAB addition in sonicated and unsonicated samples at a given initial viscosity profile. Clearly, even though earlier it was shown that their rheological properties are similar in the absence of CTAB; after addition of CTAB, the rheological properties of sonicated samples increase more due to the higher number of individual CNCs that make use of more surfactant molecules in the network formation. It can be concluded that sonication in conjunction with CTAB molecules creates an overall stronger network. It is noteworthy to mention that qualitatively behaviour for sets of samples for all CTAB concentrations is similar.

Exposing samples to higher level of sonications energy disperse the particle to smaller scales as giant initial agglomerates breaks apart further with more input of sonication energy/duration.

Figure 6, shows steady shear viscosity along side to corresponding stress that has been sketched jointly on a double logarithmic scale.

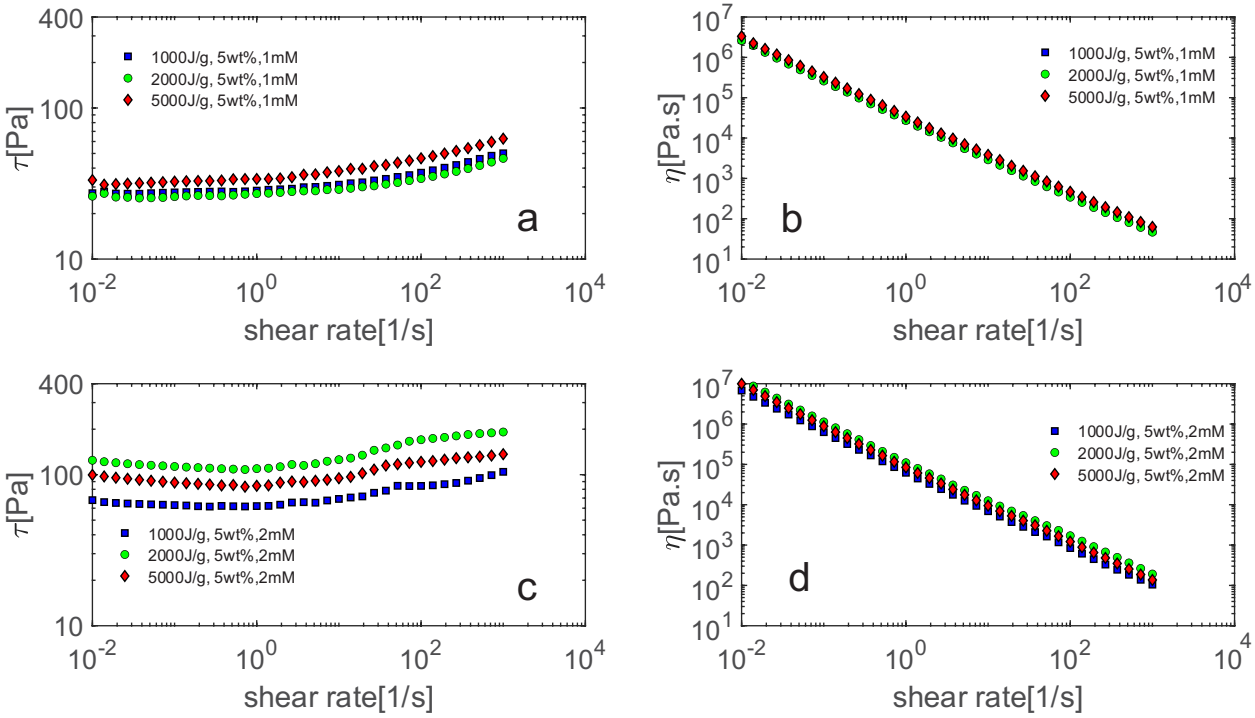

Figure 6. Steady-state shear viscosity (η), versus shear rate ($\dot{\gamma}$) for CNC suspensions 5wt% at various levels of sonication and CTAB content at 25°C sketched on double logarithmic scale.

Figure 6c and **Figure 6d** reveal that at 2mM CTAB content, increasing the sonication energy, it causes a further decreases in stress and viscosity respectively, when sonication increases from 2000 to 5000J/g.

5.5 Thixotropic behavior of CNC-surfactant gel

The rheological properties of thixotropic and shear-thinning fluids differ knowing that thixotropic materials have a dependency on shear history. Currently, the generally accepted definition adopted for thixotropic fluids, according to Mewis and Wagneris[59] the decrease of viscosity through the passage of time when a finite shear is applied to a sample that prior has been at the quiescent condition and consequent recovery of viscosity in time when the shear is stopped or decreased. At rest, the microstructure of thixotropic fluids goes through changes with time due

to Brownian motions, a phenomenon that is referred to in the literature as [60,61] To assess the thixotropic behavior of CNC-surfactant gels, initially and after the standard pre-shearing protocol, the samples were sheared from 0.01(1/s) to 100(1/s), i.e. low to high (L-H); consequently the pre-shear protocol was applied again, and the samples' shear viscosity was measured this time from 100(1/s) to 0.01(1/s), i.e. high to low (H-L). Results have been shown in sets, in **Figure 7**. **Figure 7a** shows the shear viscosity of pure CNC 5wt% sample going through the full cycle of shear described earlier. Viscosity after pre shear at 400(1/s) (comparing H-L with L-H) shows an overall increase that can be ascribed to CNC particles rearrangement and possible break up of agglomerates because of the shear application, i.e. anti-thixotropic effect. In **Figure 7**, we also observe that the addition of an increasing amount of CTAB has made the CNC-surfactant gel increasingly less thixotropic. Due to the flexible backbone of surfactant that connects neighboring CNCs together, the lower thixotropic behaviour of CNC gel as an increasing function of CTAB concentration is expected. Moreover, the rate of return of CNC particles to their original configuration due to their anisotropy also helps the structure retaining its original configuration. Estimating the rate of return of rod-like particles such as CNC can be done using orientation models originally developed by Folgar-Tucker[62]. However, discussion on kinematic of orientation and reorientation of CNC as a function of shear rate is out of the scope of this study and will not be discussed further.

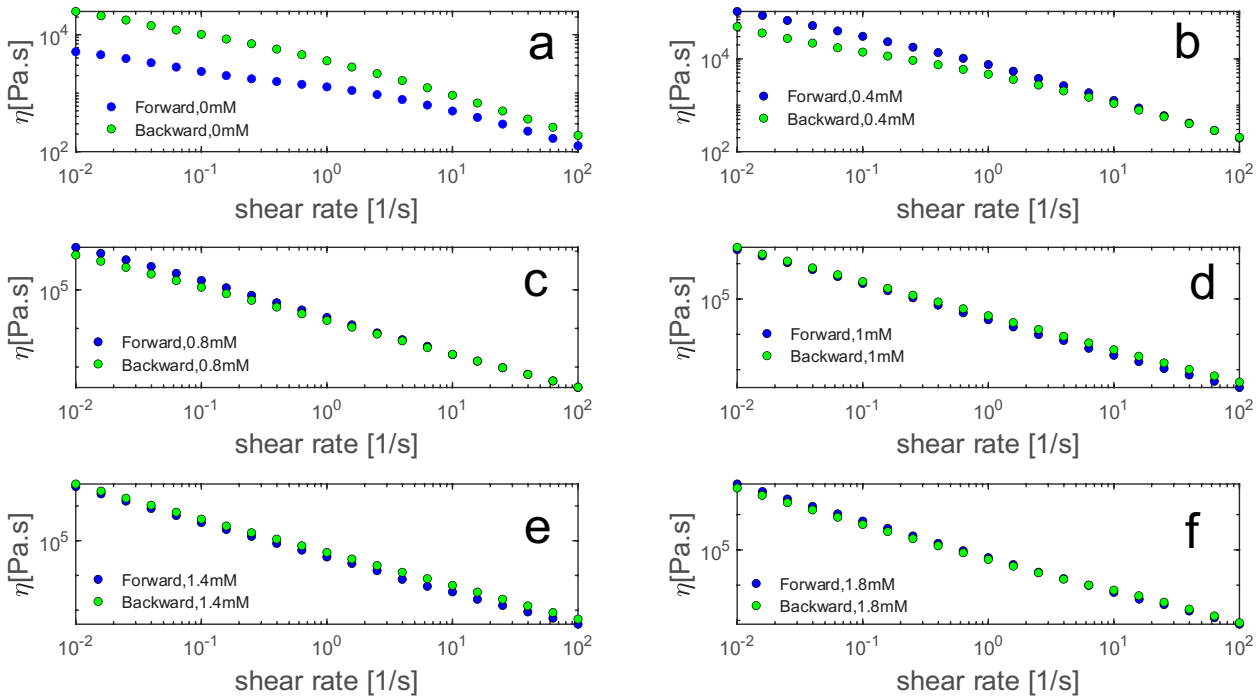

Figure 7. The shear viscosity of CNC-CTAB gel/suspension with CTAB concentration of 0-1.8mM sketched on double logarithmic scale.

5.6 Linear viscoelasticity

Figure 8 depicts the rheological frequency sweep experiments in LVE over a range of angular frequency (0.1-100rad/s). **Figure 8a** depicts the storage modulus of CNC samples in presence of different concentrations of CTAB, while **Figure 8b** depicts loss modulus as a function of frequency. Measurements have been adopted through the usage of low-to-high (L-H) shear mode. For CTAB free suspension of CNCs, G″ is greater than G′, which indicates that CNC in the absence of the surfactant, system depicts dominant viscous character. This trend follows with an overlap between G′ and G″ for suspension containing 0.2mM CTAB. 0.2mM is threshold after which, the system starts displaying viscoelastic gel like behaviour and continues to evolve by adding more CTAB as G′ becomes greater than G″ over the entire range of angular frequency. As shown in **Figure 8**, the transition from gel-like behaviour to viscoelastic solid along with the increasing gap between G′ and G″ over a range of frequency commences at 1mM CTAB; at this concentration G′ becomes completely independent from G″. Ranjbar and Hatzikiriakos's[17] LVE results for 3wt% CNC with the same amount of CTAB concentration displayed the same trend;

however, CTAB loading required to impart similar changes were higher consistent with the results presented in **Figure 5**.

Inspecting the report by Solomon et al.[50] on structural differences between homogenous and heterogenous rod fractal clusters might reveal the role played by CTAB molecules in making the system more elastic. Due to interaction of CTAB molecules with CNC surfaces, through manipulation of ionic strength of the medium and hydrophobic effects (due to, for example, attractive van der Waals or depletion forces[63]) or effect of excluded volume (due to packing[64,65]), the system falls into a regime in which interaction among particles dominate thermal forces, causes the local mobility of particles to decrease. Hydrodynamic interactions among individual CNCs also play a key role in gel formation[66,67]. The impact of packing or attractive interactions also causes the mobility of individual particles to scales down to the order of the rod's diameter. Reaching this stage, causes the system to achieve kinematic arrest, which macroscopically manifests as more elasticity and non-ergodicity. The rod's gel is tightly packed network of particles in which fully arrested dynamics has occurred due to strong attractive forces among particles. Dynamical arrest in these cases can be assimilated to traffic jam example. Individual cars in a traffic jam situation, although having the capacity to move at a faster pace than traffic, find that their movement is severely inhibited by the neighbouring cars, a situation that is most like glassy state of colloids. When the cars in such traffic are also glued to another, due to bulkiness of their overall shape (in colloidal terms, formation of a cluster due to attractive interactions between particles) their movement is slower as compared to individual cars. Both situations render the CNC network non-ergodic.

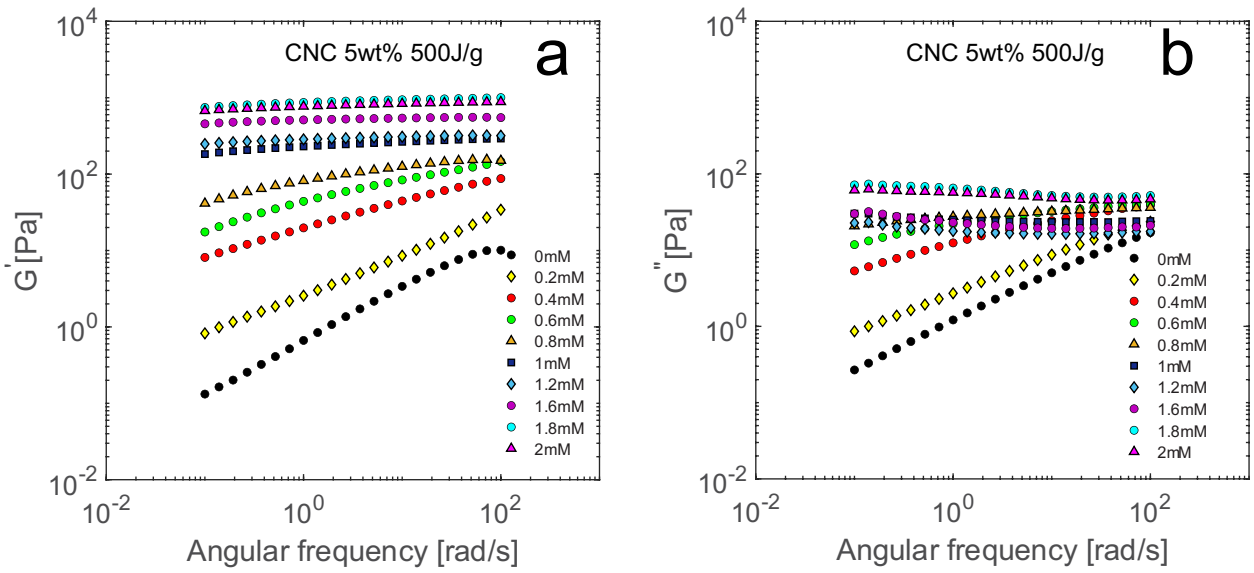

Figure 8. Linear viscoelastic characterization of CNC-CTAB solutions/gels for CNC concentration and at different CTAB concentrations. (a) Storage modulus (G'), (b) Loss modulus (G"), of CNC/CTAB solution at different CTAB concentrations for strain amplitudes of 1% using a parallel plate geometry sketched on double logarithmic scale (50 mm in diameter, 4°angle cone, and gap size of 0.5 mm) at 25˚C.

5.7 Strain amplitude sweep to determine yield stress

Figure 9 shows the strain amplitude dependence of dynamic moduli (G′ and G′′) of the 5wt% CNC (500J/g) samples containing 0-2mM of CTAB. Both storage and loss moduli are independent of the input strain amplitude in the linear viscoelastic region (LVR) (**Figure 9**). The storage modulus and loss modulus are strictly defined for LVR, and therefore their magnitudes at larger strain levels can have vague physical meanings. However, through adapting a careful analysis, the measurement of these two parameters at a fixed frequency can provide invaluable information. **Figure 9a** displays the rheological behaviour of pure 5wt% CNC sample that depicts dominant liquid-like behaviour over the entire strain amplitude sweep. In line with previous results, the value of the plateau moduli in LVR increases with the increase in CTAB concentration. In the presence of CTAB, G′ > G′′ in all cases shown (**Figures 9b-j**) a condition that in small amplitudes indicates the dominance of the solid-like behaviour for the 5wt% CNC samples because of gelation in the presence of surfactant. However, in each case beyond a critical strain amplitude γ_c, i.e., strain at which linear to nonlinear viscoelastic behaviour occurs, G′ features a dramatic

drop, while G″ experiences a slight increase to reach a maximum value (overshoot) followed by a dramatic decrease.

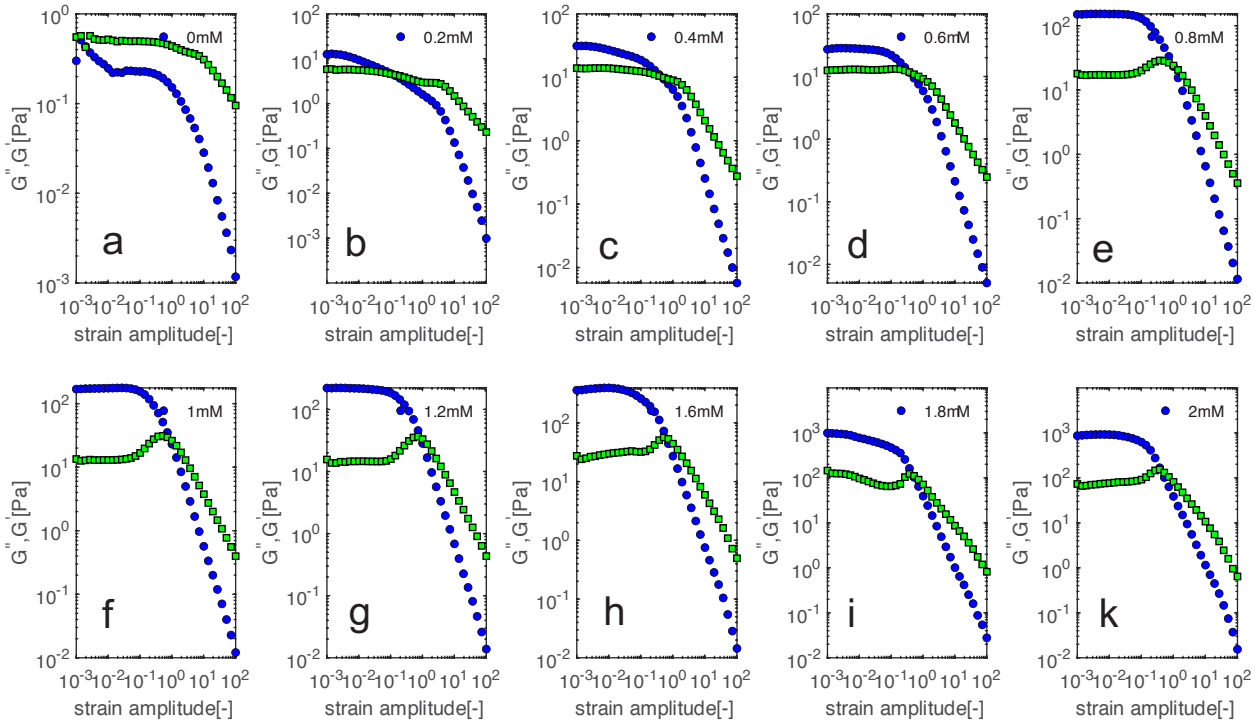

Figure 9. Oscillatory amplitude sweep response of CNC 5wt% suspensions containing different amount of CTAB (0-2mM) for strain amplitudes of γ_0=0.1-10000% at an angular frequency of ω=1 rad/s using parallel plate geometry sketched on double logarithmic scale (5 mm in diameter, 4°angle cone, and gap size of 0.5 mm) at 25˚C. Storage modulus and loss modulus has been designated with open symbol and solid symbols, respectively.

Four different types of viscoelastic nonlinearity are expected after surpassing the limit of the linear viscoelastic regime[68]. Type I stream (strain-thinning) that is observed commonly in polymer melts and suspension in which decrease of both G′ and G″ occurs in the nonlinear region as a result of reduced drag at the local level through alignment of network constituents with the flow field; Type II stream (strain-hardening) happens in cases where both G′ and G″ show increase in nonlinear regime; Type III stream (weak strain overshoot) occurs where G′ decreases, however, G″ initially increases and then decreases, and Type IV stream (strong strain overshoot) occurs where both G′ and G″ show an initial increase that is followed by a decrease.

Initially, samples up to CTAB concentration of slightly less than 1mM depict Type I stream behaviour that is common for polymer melts and suspension in which network constituents align

along the flow field. After surpassing 1mM concentration threshold, inspecting the behaviour of G′ and G″ reveals initial drop in storage modulus of the CNC-CTAB samples as a function of strain amplitude is concurrent with an initial increase in loss modulus which underscores that CNC 5wt%-surfactant samples depict the type III nonlinear viscoelastic behaviour (**Figure 9**). After overshooting of G″, the pace of decrease in G′ occurs more severely as opposed to G″ (**Figure 9b-f**). Therefore, at the vicinity of critical strain amplitude (γ_c) at each CTAB loading, G′ becomes less than G″, thus reveals solid to liquid transition because of breakage of CNC network at sufficiently large deformation. The appearance of weak strain overshoot under large amplitude oscillatory shear deformation is directly correlated to the sudden increase of energy dissipation of hydrogel experiencing dynamic deformation over large strain amplitudes. The existence of this maximum (known as the Payne effect) is an indication of the existence of yield stress. In fact a sequence of processes start at the point where G″ starts increasing (increase of dissipation showing flow initiation) that is also the point where the stress ($|G^*|$)-strain γ relationship deviates from linearity[35,69,70]. The stress at the maximum value of G″ has also been interpreted as yield stress, essentially it indicates the beginning of destruction of the self-similar interconnected clusters (**Figure 9**)[36,37,39]. The subject of yield stress will be analysed in more detail in following sections. A comparison of G″ behaviour with respect to strain amplitude in **Figure 9** also reveals that samples with CTAB concentration of more than 0.8mM display weak strain overshoot. Furthermore, gel with CTAB concentration of 1.6mM displays the sharpest increase in strain overshoot. Interpreting these experimental observations based on Sim's model[71], reveals that with the addition of CTAB above CMC, network creation rate parameters increase till 1.6mM and then displays a modest decrease. Abbasi Moud et al.[31] also observed a similar trend in their CNC-salt system, which suggests that both systems of CNC-surfactant and CNC-salt perhaps display the similar microstructures. The overshoot in G″ as a function of strain amplitude can be considered a criterion describing visco-plastic fragility[72].

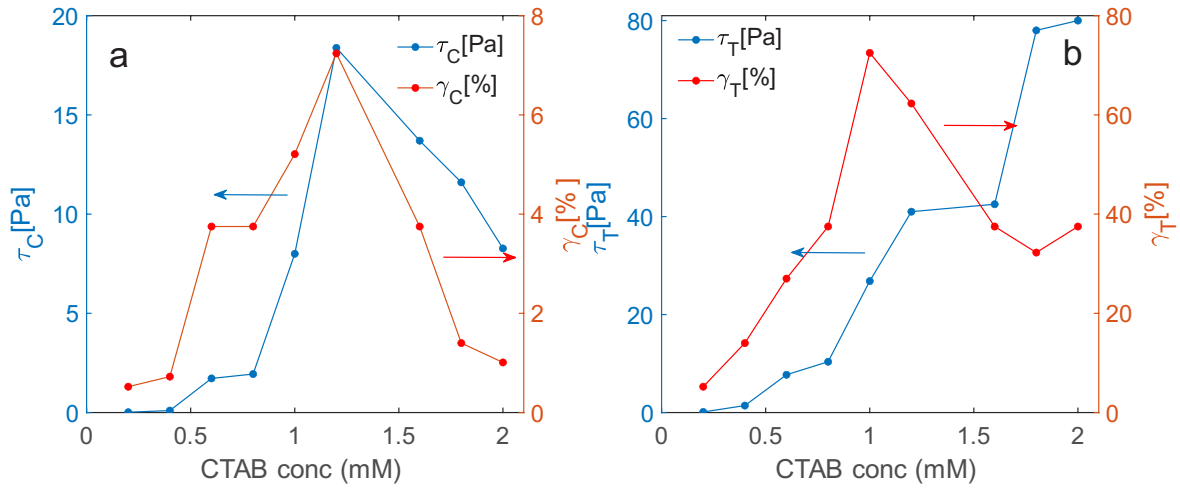

Figure 10. a) Critical strain amplitude γ_c (linear to nonlinear transition) and corresponding shear stress τ_c reflected on the right and left horizontal axis, respectively b) and crossover strain amplitude γ_T (solid to liquid transition) and corresponding shear $\boldsymbol{\tau_T}$ reflected on the right and left horizontal axis, respectively as a function of CTAB concentration.

Moreover, the strain dependence of G′ and G″ for CNC (5wt%)-CTAB (0.6,1 and 2mM) at different angular frequencies (ω = 0.5, 10.0, and 15.0rad/s) are shown in **Figure S1**. The CNC/CTAB suspensions showed type III viscoelastic behaviour at all frequencies (see **Figure S1**), indicating that the type of the inter-cycle viscoelasticity of the CNC/CTAB systems is frequency invariant.

In comparison to shear measurement, SAOS measurements are advantageous as they are non-invasive at small deformation and they cause minimum disturbance to fluid structure[73]. In the literature, there exist many ways to determine the yield stress from SAOS measurements; however, there is no consensus as to how to determine the yield stress[74]. Yield stress analysis through the analysis of critical strain amplitude γ_c and crossover strain amplitude γ_T concomitantly helps with gaining further insight into the network of CNC-surfactant gel. The crossover strain amplitude is defined as the point where G′ is equal to G″ , which is nearly the same to the strain that G" attains a maximum (i.e. where the solid-like gel flows). The critical strain amplitude (yield point) is the strain level where G′ decreases by 5% from the SAOS plateau. Between yield point and flow point, the network starts to break at the microscopic level. Above the flow point the macroscopic flow occurs due to long-range destruction of the network. Both γ_c and γ_T show increase before reaching to 1mM CTAB, i.e. the point that CTAB surfactant molecules self assembles into micellar structures (**Figure 10**). **Figure 10** depicts changes in critical strain amplitude γ_c (linear to

nonlinear transition) and crossover strain amplitude γ_T (solid to liquid transition) as a function of CTAB concentration. We observe that both graphs in the vicinity of 1mM CTAB concentrations show a maximum that is in line with previous observations that the nature of the network of CNC-surfactant is different below and above CMC. However, shear stress that depicts gradual yielding of the network from τ_c to τ_T, displays that τ_T - τ_c grow larger as more CTAB is added into the system. This comparison shows that system yield over larger strain domains when the concentration of CTAB increases.

This observation is again in line with previous results, in which we found that the addition of CTAB initially leads to network formation through bridging mostly. This trend continues until the point of CMC. We observed that increasing CTAB concentration shifts the position of both γ_c and γ_T to lower strain amplitudes (**Figure 10**) between 1mM and 2mM. This suggests that the formation of a stronger network as a result of the incorporation of more amount of CTAB into the network, that yields at smaller deformations (stiffer network)[31].

Similarly, Chen et al.[75] compared the rheological behaviour of CNCs in the aqueous solution of poly(vinyl alcohol) (PVA) with flexible backbones and carboxymethyl cellulose (CMC) with semi-rigid backbone. The authors reported type III behaviour for CNC/PVA ensemble, however CNC/CMC displayed type I stream. They suggested that the display of type III behaviour for the CNC/PVA system originates from the aggregated structure of CNC through adsorption of PVA chains and simultaneous bridging effect. However, we believe in our CNC-surfactant system with the same level of backbone flexibility, the formation of semi-stable structural complexes in medium strain amplitudes causes the appearance of weak overshoot in G″ versus strain amplitude diagram (shear-induced structures[72]). This could be attributable to the decrease in the inter-particle mean distance in suspension/cluster system through the application of shear force, thereby, facilitating the network formation and leading to the formation of larger load-bearing junctions (physical bonds). Brownian dynamic simulations of Moghimi et al.[38] indicates that the structure heals faster due to rearrangement of particles at low shear rates. In fact, an imposed shear flow provides an external driving forces that accelerate local movements, including cluster and individual particle rearrangements. It was observed that for low strain amplitude, oscillatory shear induces short-range rearrangements inside the structure that increase the number of bonds over

time, but the process does not change the structure significantly. In this shear regime, shear helps the structures to heal more quickly.

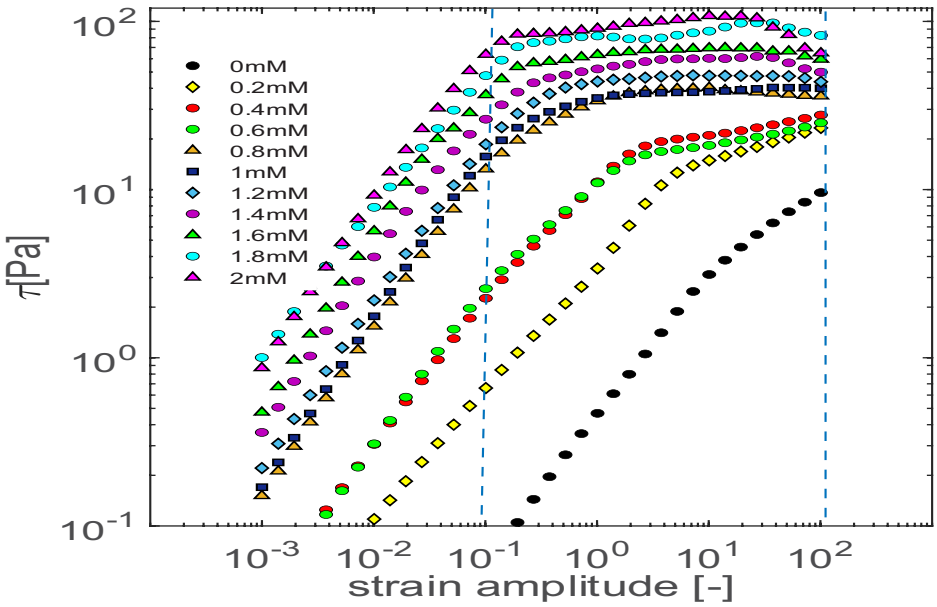

Figure 11. Oscillatory amplitude sweep response of CNC 5wt% suspensions containing different amount of CTAB (0-2mM) for strain amplitudes of γ_0=0.1-10000% at an angular frequency of ω=1 rad/s using parallel plate geometry sketched on double logarithmic scale (50 mm in diameter, 4°angle cone, and gap size of 0.5 mm) at 25˚C. The dashed line approximately designates the area in which yielding occurs.

Figure 11 shows the shear stress as a function of strain amplitude sketched for samples with CTAB concentration, ranging from 0-2mM for strain amplitudes of 0.01-10000%. Generally, the attractive forces in simple fluids start to modify the stress response of the fluid when the strength adhering particles to one another is strong enough to cause a dynamical arrest. In such cases, a 3-D percolated network will form that coincides with the appearance of yield stress[76]. In CNC-CTAB network appearance of such a percolated network occurred when CTAB concentration surpassed 0.2mM (See **Figure 9a**) as sample with 0mM CTAB content in **Figure 11** displayed no yielding point. Only after increasing CTAB content to 0.2mM, an apparent plateau appears in shear stress versus strain amplitude. Criterion to differentiate between yielding and unyielding zone, is knowing that the rate of deformation of the sample is almost constant in the unyielded zone, i.e., the stress ascends linearly with the applied strain, a well accepted signature for elastic solid deformation regime (see the part of curves before the first dashed vertical line in **Figure 11**). After increasing the CTAB concentration to higher loading levels, the system displays a complex

behaviour, i.e. appearance of a wide plateau, perhaps depicting local weak maxima implying double yielding behaviour. Based on evidences presented here, it can be concluded that at high CTAB concentrations (>1.6mM), CNC-CTAB network behaves as an attractive gel with appearance of two yielding point corresponding to the formation of a 3-D network of CNC clusters (two apparent local maxima appear in Figure 12 at the highest CTAB concentrations). The first yield point is related to restructuring within the gel network, that enables the gel constituent (cluster and individual particles) to flow past one another. The second yield stress is related to extended demolishing of clusters with shear that leads to formation of a more homogenous suspension. The second yield stress appearance diminishes at lower CTAB content (concentrations less than 0.6mM) as there is enough free volume for clusters to have freedom to pass each other and flow[50,51] . It also stands out that increasing the CTAB content leads to extension of the yielding region and appearance of strain stiffening region for particularly samples with CTAB concentration of more than 1mM. Similar nonlinear behaviour was recently observed by Abbasi Moud et al.[31] for a similar system of CNC based hydrogel. We can also infer, knowing that there is a difference between structure formed in CNC-CTAB hydrogel below and above CMC, that even below CMC, percolated network has a measurable yield stress.

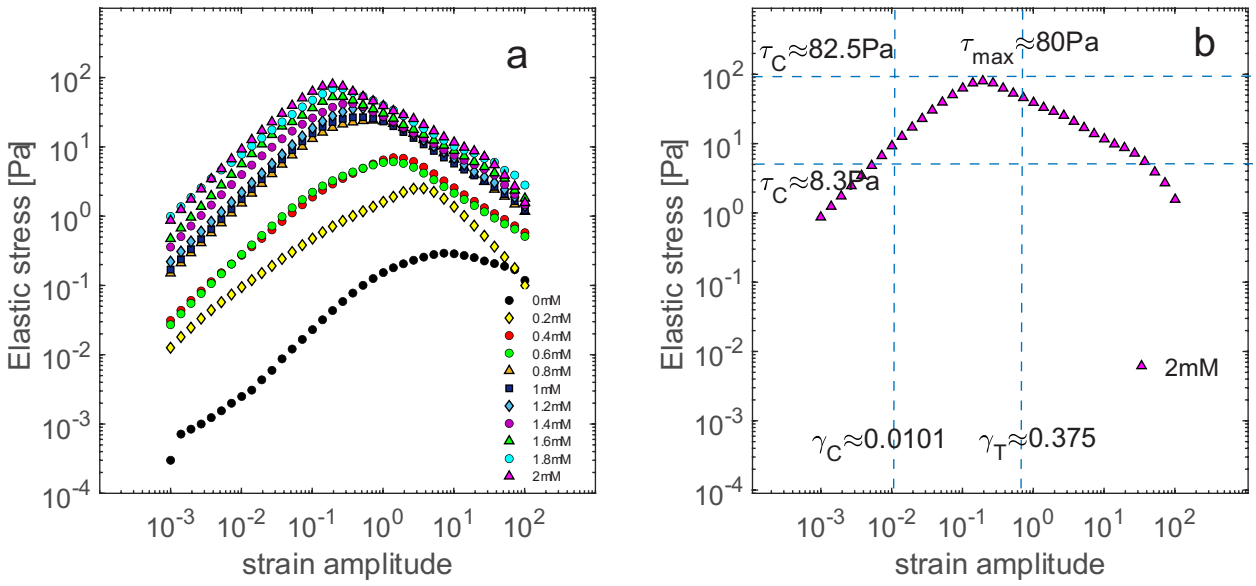

Figure 12. Oscillatory amplitude sweep response of CNC 5wt% suspensions containing different amount of CTAB (0-2mM) for strain amplitudes of γ_0=0.1-10000% at an angular frequency of ω=1 rad/s using parallel plate geometry sketched on double logarithmic scale (50 mm in diameter, and gap size of 0.5 mm) at 25˚C.

Table 1. Yield stress analysis obtained through oscillatory and steady shear experiments. The determination of yield stress using Herschel-Bulkley model as a function of CTAB concentration determined from the flow curves by the low-to-high (L-H) and high-to-low (H-L) shear rate test modes.

CTAB conc.[mM]	T_c [Pa]	T_T[Pa]	T_{max} [Pa]	$T_{Herschel\text{-}Bulkley}$ [Pa] Static yielding (95% confidence bounds)	$T_{Herschel\text{-}Bulkley}$ [Pa] Dynamic yielding (95% confidence bounds)
0.2	0.02	0.5	2.52	0.4(0.3, 0.6)	0.3(0.2,0.4)
0.4	0.1	3.6	6.1	0.9(0.6,1.2)	0.8(0.5,1.1)
0.6	1.7	7.3	7	4.3(2.6, 5.9)	3.5(2.7,4.2)
0.8	1.9	20.2	24.2	12(9.6, 14.3)	7.8(6.8, 8.9)
1	8	29.9	26.7	25.1(24.8, 26.7)	29.1(28.7,29.6)
1.2	18.4	42	36	32.3(31.5,33.2)	37.6(37.4,37.9)
1.4	13.1	49.1	42	33.6(32.7,34.5)	42(41.5,42.5)
1.6	13.7	50.9	52.6	40.3(39.4,41.3)	53.7(53,54.4)
1.8	11.6	78.4	69.3	60.9(59.1,62.7)	51.8 (51.7,52.2)
2	8.3	82.5	80	53.5(52.3,54.7)	51.8(51.3,52.3)

Yielding in systems such as CNC-CTAB hydrogel network is complex. It has been demonstrated experimentally that flow in amorphous matter, happens at the macroscopic scales in localized zones. In fact, the existence of such zones has been reported in the literature, for the systems that are sheared extremely slowly in computer simulations or confocal microscopy experiments[77–79]. It has been observed that yielding occurs, mostly in the zones with lower number of particles that leads to larger scale irreversible reconfigurations[77–79] Authors believe, same microstructural reconfigurations occur in CNC-CTAB gel once the system experience a certain threshold of strain or stress. In line with these studies, Donley et al.[72] in a recent paper has shown that overshoot in the loss modulus, a phenomenon associated with plasticity and yielding, also known as *Payne effect*, is due to the continuous transition from recoverable to unrecoverable strain from small to

large strain amplitudes. It is obvious based on **Figure 11**, that there is no single yield point in CNC-CTAB network, when specially CTAB content is more than 0.8mM, versus strain amplitude. In fact, it appears there exist a continuum of rheological responses between the unyielded and yielded samples. It appears that the traditional interpretation of solid like and plastic dissipation are vague and oversimplified and a definition based on energy is more logical[74]. In fact, the loss modulus is a composite parameter, that reflects both the fluid element and viscoelastic solid element contributions. Binary yielding models, such as Bingham[80,81], Herschel and Bulkley[82] are only approximation of the steady state behaviour and need proper adjustment to take into account the concept of transient yielding. In the absence of an external driving forces, microstructural elements of the gel are trapped in energy potential wells with different heights. If the applied energy, is less than a certain threshold, here $E< E_1$, the flexible structural constituent of the gel will enter an extended state without alteration of the structure. When the force is removed, the material maintains its pre-shear structure and structure at macro level and behaves as an elastic solid. When the applied energy is in an intermediate level, here $E_1<E<E_2$, energy break the structure, however the input energy is still weak enough for the particle to rearrange in a different configuration. When the energy input is higher than a certain threshold, here $E>E_2$, probability of recombining of constituent is small and the system breaks down and flows. Energy cantered outlook of a yielding system is called multiple energy landscapes and has been discussed previously in the work of Sollich and Sollich et al[83,84].

The crossover of G' and G'' has been used previously as one estimate of yield stress[85] (previously labelled as τ_T) and initial point of yielding τ_c also can be used as the second estimate of yield stress. Furthermore, the dynamic stress data can also be remodelled as the elastic component of stress (G' multiplied by the absolute strain and sketched against strain). The maximum in such curve can also be interpreted as yield stress and here labeled as τ_{max} [86] and shown in **Figure 12**. Ascending trend before the maximum point conforms well with expectations as increase in strain amplitudes means higher Weissenberg number and more domination of elastic forces in comparison to viscous forces. The lines in **Figure 12b**, represents yield strain and stress obtained through oscillatory strain sweep experiment. **Table 1** shows results of comparison from different methods used in determining yield stress of CNC-CTAB network. It appears that at the lower

CTAB contents, τ_{max} falls out of the range of yield stress defined by τ_c and τ_T; however, at higher CTAB content it is very well positioned in the pre-determined range.

Due to thixotropic behavior of the sample until 0.8mM CTAB content a single yield stress value cannot be extracted from shear ramp experiments (**Figures 4a** and **4b**). Indeed two distinct yield stresses can be found as previously reported by Mujumdar et al[87] for fluids that display thixotropic behavior. Initially, a static yield stress can be determined through fitting of the Herschel-Bulkley model on flow curve data from low shear rate to higher shear rate, and a dynamic yield stress that is result of fitting the same model on the flow curve when shear rate is descending from high to low shear rates. In all cases, the static yield stress is generally higher than dynamic yield stress as static yield stress is confounded with viscoelastic effects prior to material's yielding[88]. However, for samples with CTAB content of 1-1.6mM dynamic yielding was found to be slightly higher than static yielding, due to possible more favourable quick arrangement of gel constituents after gel break up during pre-shear experiment, and absence of thixotropic effects.
One of the most elementary models capturing yield stress fluid's behaviour is the Herschel-Bulkley model:

$$\sigma \geq \sigma_y \Rightarrow \sigma = \sigma_y + K\dot{\gamma}^n \qquad [1]$$

Where σ_y represents yield stress of the fluid, and K and n are the model parameters. Fitting this equation to **Figure 4c** and **4d**, leads to the last two columns in **Table 1** that represent yield stress obtained from fitting equation 1 on data displayed in **Figures 4c** and **4d**. As it appears, static and dynamic yield stress predicted by the Herschel-Bulkley equation is very well in the range of yield stresses predicted through oscillatory experiments. Yield stress extracted from cross over of G' and G'' is higher than yield stress obtained from Herschel-Bulkley model as equality of G' and G'' indicates that there has been a significant amount of dissipation, therefore, material should have yielded prior to this point[89]. Experimentally, Herschel-Bulkley has been seen to fit the experimental data successfully well over several decades of shear rates in case of emulsions, foams and microgels with acceptable level of reproducibility[90]. However, this method of yield stress determination suffers from a few limitations. First wall slip can impact flow at low shear rates; second, time dependent phenomena such as thixotropy impact the shape of flow curve and its extrapolation depend at low shear rates on the pace that the shear rate is swept[91] and; finally this

method of yield stress determination is subjected to fitting protocol, exclusion of outliers, initial flow instabilities and resolution of the rheometer. Readers are encouraged to read the report of Dinkgreve et al[89] for more thorough discussion on strong points and shortcoming of various methods aimed at determining yield stress of complex fluids. Moreover, as it was shown in **section 3.4**, CNC-CTAB network almost loses its thixotropic behavior after addition of 0.8 mM CTAB. This phenomenon can be seen in convergence of static yield stress and dynamic yield stress calculated in **Table1**. The different behavior of CNC-CTAB in convergence of yield stress below and above CMC, again shows that network is microstructurally different. Mewis and Spaull[92] suggested that yielding occurs at a certain shear strain, as opposed to a certain yield stress. In that case, $[\gamma_c(\text{min})\ \gamma_T\ (\text{max})]$ can also be defined to locate the bounds on the strain required to yield the hydrogel structure.

5.8 Relating steady and oscillatory shear for yield stress measurements

To create a connection between oscillatory and steady shear experiment's yield stress analysis, **Figure 13** was sketched[93]. **Figure 13** shows the same data as **Figure 4**; however, the viscosity is depicted against shear stress. The dashed lines in **Figures 13a** and **13b**, indicates visually segments of the curves, at which viscosity goes toward infinity. To illustrate the yielding transition, curves in **Figures 13c** and **13d** has been divided into 3 distinct regions, i.e. I, II and III, representing initial yielding point, apparent plateau, and second yield point, respectively. Same analysis can be applied to data of sample with CTAB content of 1.8mM. Sample containing 1.8mM displays narrower yielding in L-H experiment; however, 2mM samples shows the exact opposite trend. However, samples with lower CTAB contents does not show double yielding transition, therefore, existence of double yielding can be interpreted as a structure that is more complex and heterogenous locally and globally as compared to samples with one yielding point. The region II can be interpreted as cascade of stepwise yielding that is correlated to micro-yielding of localized zones with different energy depth as described earlier. As expected, yield stress behaviour for steady shear matches well with the data obtained through oscillatory analysis of yield stress, in which, samples with higher CTAB content of 1.6mM show double yielding behaviour. Another interesting point is appearance of double yielding for 1.8mM and 2mM samples during H-L flow (See **section 3.4**) that shows aging of the sample has led to complete reconstruction of the network

as CNC-CTAB hydrogel almost present identical linear and nonlinear rheological behaviour. One shortcoming of steady shear experiment is their inadequacy to show yielding region akin to oscillatory experiments as aside from 1.6-2mM samples, samples with CTAB content of 0.2-1.6mM only show one single yield stress. It appears that oscillatory experiments are richer and provides a clearer picture of yielding transition as opposed to steady shear experiment. A point of consistency, found between results of **Figure 11** and **Figure 13c-d**, is the width of yielding region that is consistently sharper for 1.8mM sample in comparison to 2mM. Moreover, oscillatory method of yield stress assessment share similarity with dynamic yield stress of steady shear experiment as both are labelled as dynamic yield stress[94]. Aligned with expectations, considering data of **Table1**, it appears that τ_c and τ_T can successfully fully define the yielding region and be considered a global criterion describing yielding transition. In fact, the yielding region can be expected to be bounded by τ_c and τ_T as [τ_c(min) τ_T (max)], regardless of yielding assessment criteria.

During start up flow experiment, with the help of Brownian dynamics, Moghimi and Petekidis[95], examined the effect of attraction strength and range of attraction on the yielding transition of colloidal glasses, a study adaptable to current report as CTAB concentration influences both the attraction strength and range of attraction. The initial rise in stress was correlated to energy storage of the system, while second peaks were related to energy dissipation through cage melting and plastic flow[96,97]. When a strong short-ranged attraction was added, an additional second yield stress appeared at lower strain in both experiment and Brownian dynamics simulation. They also observed the shift in stress peak to lower strains due to having stronger attraction between particles leading to localization. Furthermore, in experiments, the location of second maxima extended to larger strain with inclusion of attraction between particles, aligned with previous experiments[36,39]. In our experiments we see the appearance of two yield points after the addition of 0.8mM CTAB; however, steady shear only shows two yield stress after CTAB reaches 1.8-2mM. The position of the second peak also extends to higher strains as more CTAB is added and stress requires for appearance of second peaks is higher, i.e. an indication of strain stiffening that also implies that cluster deformation takes more stress than breaking the links between clusters.

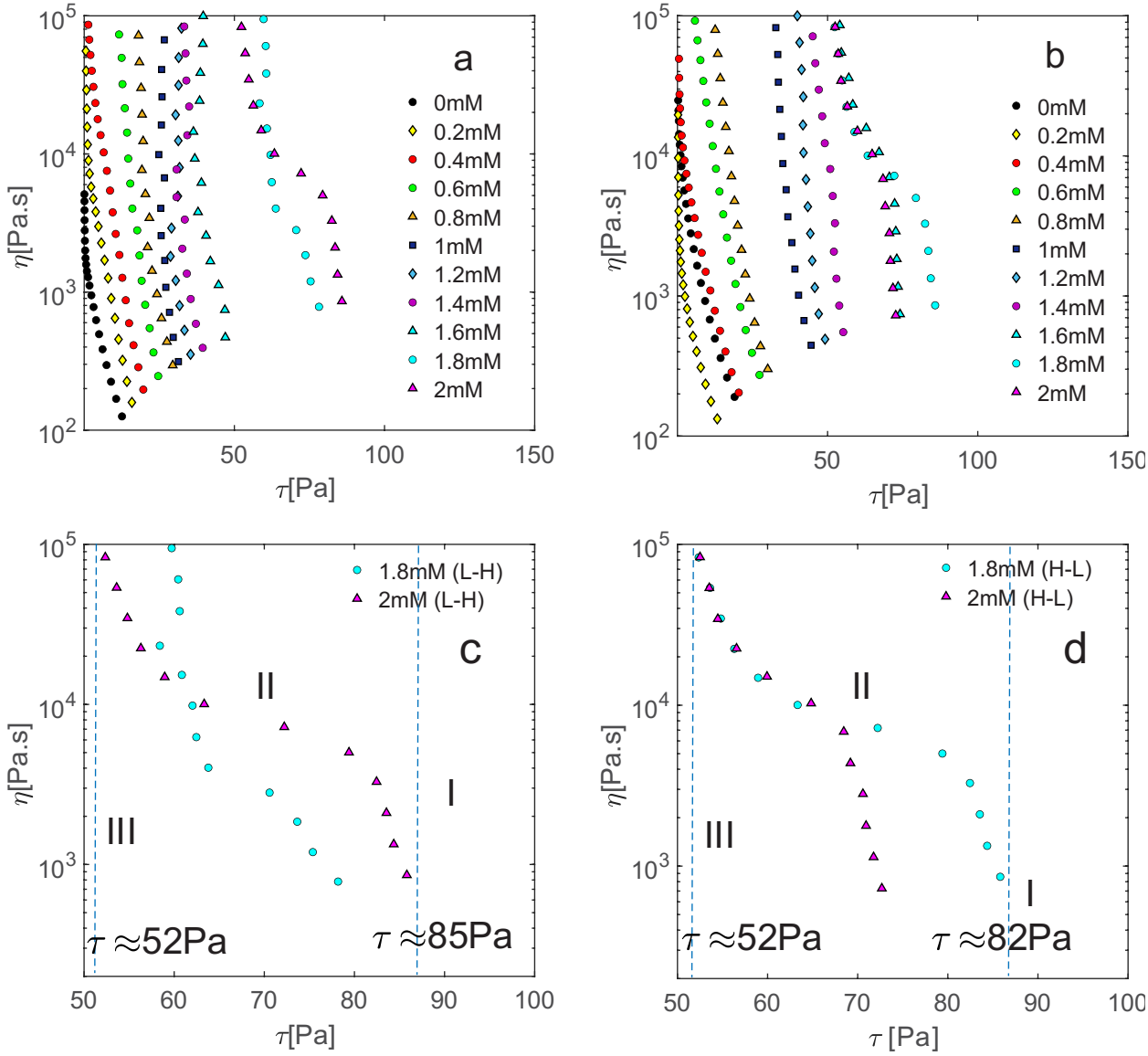

Figure 13. The shear viscosity of CNC-CTAB gel/suspension with CTAB concentration of 0-2mM sketched on double logarithmic scale (a: η vs τ (L-H), b: η vs τ (H-L), c: η vs τ (L-H) and d: η vs τ (H-L) as a function of shear stress. The set of pictures of c and d re present same data of a and b but only when the samples are restricted to 1.8mM and 2mM samples. Dashed lines represent asymptotic lines showing point at which viscosity approximately goes towards infinity.

5.9 Creep tests for yield stress

Creep testing was used to investigate the yield stress behaviour of hydrogels[98] as a validatory experiment for CTAB content of 1mM. **Figure 14** shows the resulting strain as function of various level of applied stress from 10-50Pa. The range of stress was chosen to include the yielding stress values obtained earlier in **Table1**. Based on **Table1**, the sample with 1mM CTAB

yields between 8 and 29.9Pa; therefore, levels of stressed chosen for creep experiment might reveal the validity of the yield stresses obtained earlier. In **Figure 14**, in the intermediate levels of stress samples in addition to recovered strain showed unrecovered strain that is correlated to passage over yield stress of the material. For instance, at the end of recovery stage, for samples creeped under stress of 30Pa the accrued strain was 71.4. Therefore, accumulation of 71.4 over period of 300s, even though at a slow rate, implies that yielding based on creep experiments, started at 30Pa, and continued between 30-50Pa, in agreement with results of **Table1**. For large stresses, >37Pa, the hydrogel is completely fluidized, and the deformation rapidly increases much faster than viscous flow.

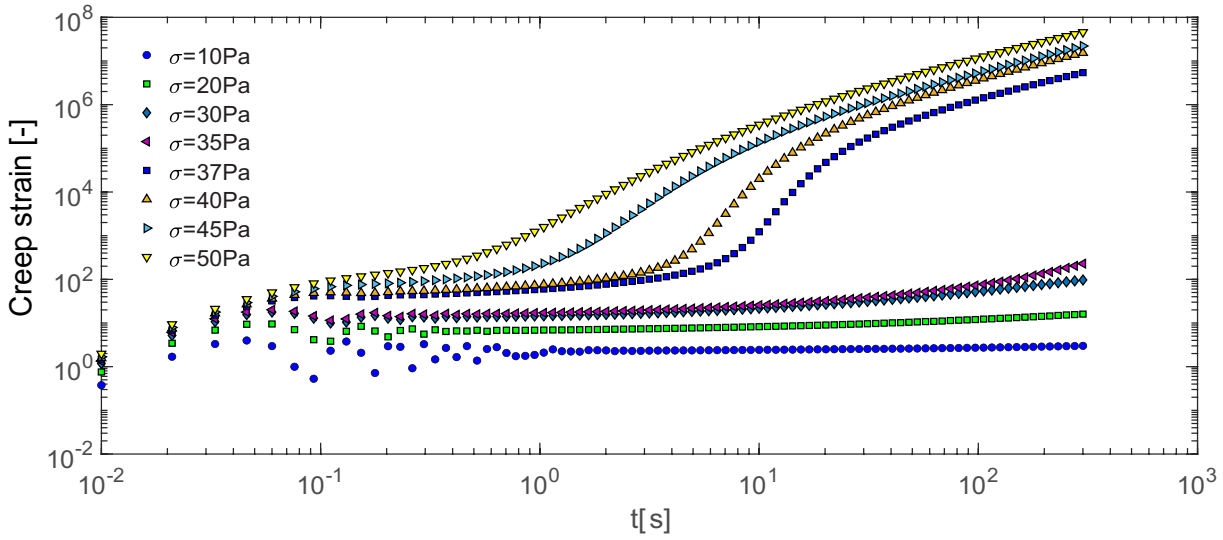

Figure 14. Creep recovery experiment of CNC 5wt% suspensions containing 1mM CTAB as a function of time using parallel plate geometry sketched on double logarithmic scale (50 mm in diameter, 4°angle cone, and gap size of 0.5 mm) at 25˚C.

Chapter 6: Conclusions and Recommendations for future work

In conclusion, employing zeta potential measurements and rheology, we probed gelation and rheological characteristics of CNC suspensions in the presence of CTAB. Results primarily point to two different network structure of CNC below and above CMC of CTAB. Below CMC, CNC-surfactant network is loosely connected by bridges formed through surfactant-surfactant interactions, however, above CMC, network structure becomes stronger as charge screening of surfactant micelles becomes the dominant mechanism driving gel formation of CNCs. CNC-CTAB gels showed shear-thinning behaviour and analysis of linear viscoelastic properties of the gel showed that after addition of 0.2mM CTAB to CNC suspension, G′ becomes greater than G″ over the entire range of angular frequencies. Transitioning from gel-like behaviour to viscoelastic solid-like behaviour along with the increasing gap between G′ and G″ over a range of frequency commences at 1mM CTAB; at this concentration G′ becomes completely independent from G″. Adding more CTAB into the gel did not change the storage modulus noticeably after 1mM. Thixotropic behaviour analysis through shear ramps revealed that inclusion of CTAB as flexible moieties decreased thixotropic behaviour of CNC gel. Strain sweep experiments revealed two distinct microstructures below and above CMC of CTAB. Below CMC, critical strain amplitude γ_c and crossover strain amplitude γ_T showed ascending trend with an increase in CTAB concentration; however, after reaching to CMC, due to formation of a stronger network, γ_c and γ_T decreased. Later we did an analysis on yield stress of CNC-CTAB gels using strain amplitude sweep stress response, results showed that CNC-CTAB network displays initially after addition of CTAB a network that has only one yield stress; however, after addition of 1mM CTAB, two yield points appears. We came to conclusion that oscillatory mode of probing yield stress of CNC-CTAB hydrogel is a clearer and richer technique for assessing yielding behaviour of the hydrogel as compared to standard fitting of binary yielding models to viscosity versus shear data. We also found that global yielding region bounded by τ_c and τ_T as [τ_c(min) τ_T (max)] can well put a bound on yielding region in terms of stress required to cause irreversible damage to the hydrogel structure. In parallel, yield strain as [γ_c(min) γ_T (max)] can also be defined to target the strain required to yield the hydrogel structure. We also probed nonlinear rheological behaviour of CNC-CTAB hydrogels at different frequencies and found that response of the system is frequency invariant. As a recap, it was found, as is the case in many soft materials, instead of having a jump, single point

structural breakup, the yielding process happens across a wide range of stresses and it is impossible to define a single yield stress. Overall, rheology was found to be a versatile technique to assess the evolving microstructure of CNC-CTAB gel.

As recommendations for future work the following are proposed.

1. The above work can be repeated by using a negatively charged surfactant (SDS) to compare the relative effects with those of CTAB.
2. It will be interesting to study the synergistic effects of electrolytes (NaCl) with those of surfactants (CTAB or SDS)
3. It has been observed in some cases that the experimental data implies the presence of a two-step yield process. More concincing experiments are needed to study this.
4. Suspensions are subject to slip effects that is apparent slip close to interfaces due to thermodynamically driven particles away from the interface. Such effects need to be assessed thoroughly in order to recover the true rheological response of these materials.

References:

1. Tsioptsias C, Stefopoulos A, Kokkinomalis I, Papadopoulou L, Panayiotou C. Development of micro-and nano-porous composite materials by processing cellulose with ionic liquids and supercritical CO 2. *Green Chem*. 2008;10(9):965-971.
2. Chawla PR, Bajaj IB, Survase SA, Singhal RS. Microbial cellulose: fermentative production and applications. *Food Technol Biotechnol*. 2009;47(2):107-124.
3. Costa SM, Mazzola PG, Silva JCAR, Pahl R, Pessoa Jr A, Costa SA. Use of sugar cane straw as a source of cellulose for textile fiber production. *Ind Crops Prod*. 2013;42:189-194.
4. Joly N, Granet R, Branland P, Verneuil B, Krausz P. New methods for acylation of pure and sawdust-extracted cellulose by fatty acid derivatives—Thermal and mechanical analyses of cellulose-based plastic films. *J Appl Polym Sci*. 2005;97(3):1266-1278.
5. Edgar KJ, Buchanan CM, Debenham JS, et al. Advances in cellulose ester performance and application. *Prog Polym Sci*. 2001;26(9):1605-1688.
6. Wang H, Gurau G, Rogers RD. Ionic liquid processing of cellulose. *Chem Soc Rev*. 2012;41(4):1519-1537.
7. Updegraff DM. Semimicro determination of cellulose inbiological materials. *Anal Biochem*. 1969;32(3):420-424.
8. Ohno H, Fukaya Y. Task specific ionic liquids for cellulose technology. *Chem Lett*. 2009;38(1):2-7.
9. Ranjbar D. Rheology and dye adsorption of surfactant-cellulose nanocrystal complexes. Published online 2019.
10. Sasaki M, Kabyemela B, Malaluan R, et al. Cellulose hydrolysis in subcritical and supercritical water. *J Supercrit Fluids*. 1998;13(1-3):261-268.
11. Dufresne A. *Nanocellulose: From Nature to High Performance Tailored Materials*. Walter de Gruyter GmbH & Co KG; 2017.
12. Carreño NL V, Labidi J. Cellulose Nanocrystal Membranes as Excipients for Drug Delivery Systems. Published online 2016:1-15. doi:10.3390/ma9121002
13. Domingues RMA, Gomes ME, Reis RL. The potential of cellulose nanocrystals in tissue engineering strategies. *Biomacromolecules*. 2014;15(7):2327-2346.
14. Hamad WY, Hu TQ. Structure–process–yield interrelations in nanocrystalline cellulose extraction.

Can J Chem Eng. 2010;88(3):392-402.

15. Online VA, Eyley S, Thielemans W. Surface modi fi cation of cellulose nanocrystals. Published online 2014:7764-7779. doi:10.1039/c4nr01756k
16. Shafiei-Sabet S, Hamad WY, Hatzikiriakos SG. Rheology of nanocrystalline cellulose aqueous suspensions. *Langmuir*. 2012;28(49):17124-17133.
17. Ranjbar D, Hatzikiriakos SG. Effect of ionic surfactants on the viscoelastic properties of chiral nematic cellulose nanocrystal suspensions. *Langmuir*. Published online 2019.
18. Gong X, Wang Y, Zeng H, Betti M, Chen L. Highly porous, hydrophobic, and compressible cellulose nanocrystals/poly (vinyl alcohol) aerogels as recyclable absorbents for oil–water separation. *ACS Sustain Chem Eng*. 2019;7(13):11118-11128.
19. Danesh M, Mauran D, Hojabr S, Berry R, Pawlik M, Hatzikiriakos SG. Yielding of cellulose nanocrystal suspensions in the presence of electrolytes. *Phys Fluids*. 2020;32(9):93103.
20. Karimian A, Parsian H, Majidinia M, et al. Nanocrystalline cellulose: Preparation, physicochemical properties, and applications in drug delivery systems. *Int J Biol Macromol*. Published online 2019.
21. Neto WPF, Silvério HA, Dantas NO, Pasquini D. Extraction and characterization of cellulose nanocrystals from agro-industrial residue–Soy hulls. *Ind Crops Prod*. 2013;42:480-488.
22. Smole MS, Hribernik S, Kurečič M, Krajnc AU, Kreže T, Kleinschek KS. Cellulose nanofibres. In: *Surface Properties of Non-Conventional Cellulose Fibres*. Springer; 2019:61-71.
23. Balea A, Blanco A, Negro C. Nanocelluloses: natural-based materials for fiber-reinforced cement composites. A critical review. *Polymers (Basel)*. 2019;11(3):518.
24. Gerberich WW, Jungk JM, Mook WM. The Bottom-Up Approach to Materials by Design. In: *Nano and Microstructural Design of Advanced Materials*. Elsevier; 2003:211-220.
25. Hunter RJ. *Zeta Potential in Colloid Science: Principles and Applications*. Vol 2. Academic press; 2013.
26. Starritt HC, Duck FA, Humphrey VF. Forces acting in the direction of propagation in pulsed ultrasound fields. *Phys Med Biol*. 1991;36(11):1465.
27. Shafeiei-Sabet S, Hamad WY, Hatzikiriakos SG. Influence of degree of sulfation on the rheology of cellulose nanocrystal suspensions. *Rheol Acta*. 2013;52(8-9):741-751.
28. Sahlin K, Forsgren L, Moberg T, Bernin D, Rigdahl M, Westman G. Surface treatment of cellulose nanocrystals (CNC): effects on dispersion rheology. *Cellulose*. 2018;25(1):331-345.

29. Revol J-F, Godbout L, Dong X-M, Gray DG, Chanzy H, Maret G. Chiral nematic suspensions of cellulose crystallites; phase separation and magnetic field orientation. *Liq Cryst*. 1994;16(1):127-134.
30. Sun B, Hou Q, Liu Z, Ni Y. Sodium periodate oxidation of cellulose nanocrystal and its application as a paper wet strength additive. *Cellulose*. 2015;22(2):1135-1146.
31. Moud AA, Kamkar M, Sanati-Nezhad A, Hejazi SH, Sundararaj U. Nonlinear viscoelastic characterization of charged cellulose nanocrystal network structure in the presence of salt in aqueous media. *Cellulose*. 2020;27(10):5729-5743.
32. Lenfant G, Heuzey M-C, van de Ven TGM, Carreau PJ. A comparative study of ECNC and CNC suspensions: effect of salt on rheological properties. *Rheol Acta*. 2017;56(1):51-62.
33. Prathapan R, Thapa R, Garnier G, Tabor RF. Modulating the zeta potential of cellulose nanocrystals using salts and surfactants. *Colloids Surfaces A Physicochem Eng Asp*. 2016;509:11-18.
34. Shafiei-Sabet S, Hamad WY, Hatzikiriakos SG. Ionic strength effects on the microstructure and shear rheology of cellulose nanocrystal suspensions. *Cellulose*. 2014;21(5):3347-3359.
35. Bonn D, Denn MM, Berthier L, Divoux T, Manneville S. Yield stress materials in soft condensed matter. *Rev Mod Phys*. 2017;89(3):35005.
36. Koumakis N, Petekidis G. Two step yielding in attractive colloids: transition from gels to attractive glasses. *Soft Matter*. 2011;7(6):2456-2470.
37. Laurati M, Egelhaaf SU, Petekidis G. Nonlinear rheology of colloidal gels with intermediate volume fraction. *J Rheol (N Y N Y)*. 2011;55(3):673-706.
38. Moghimi E, Jacob AR, Koumakis N, Petekidis G. Colloidal gels tuned by oscillatory shear. *Soft Matter*. 2017;13(12):2371-2383.
39. Pham KN, Petekidis G, Vlassopoulos D, Egelhaaf SU, Poon WCK, Pusey PN. Yielding behavior of repulsion-and attraction-dominated colloidal glasses. *J Rheol (N Y N Y)*. 2008;52(2):649-676.
40. Pham KN, Petekidis G, Vlassopoulos D, Egelhaaf SU, Pusey PN, Poon WCK. Yielding of colloidal glasses. *EPL (Europhysics Lett*. 2006;75(4):624.
41. Chan HK, Mohraz A. Two-step yielding and directional strain-induced strengthening in dilute colloidal gels. *Phys Rev E*. 2012;85(4):41403.
42. Mohraz A, Solomon MJ. Orientation and rupture of fractal colloidal gels during start-up of steady shear flow. *J Rheol (N Y N Y)*. 2005;49(3):657-681.

43. Ahuja A, Pappas I, Potanin A. Relation between structure and stability of toothpaste with two-step yielding. *Rheol Acta*. 2020;59(3):133-145.
44. Ahuja A, Gamonpilas C. Dual yielding in capillary suspensions. *Rheol Acta*. 2017;56(10):801-810.
45. Fernández-Toledano JC, Rodríguez-López J, Shahrivar K, et al. Two-step yielding in magnetorheology. *J Rheol (N Y N Y)*. 2014;58(5):1507-1534.
46. Segovia-Gutiérrez JP, Berli CLA, De Vicente J. Nonlinear viscoelasticity and two-step yielding in magnetorheology: A colloidal gel approach to understand the effect of particle concentration. *J Rheol (N Y N Y)*. 2012;56(6):1429-1448.
47. Zakani B, Grecov D. Yield stress analysis of cellulose nanocrystalline gels. *Cellulose*. Published online 2020:1-17.
48. Kushan E, Demir C, Senses E. Surfactant Driven Liquid to Soft Solid Transition of Cellulose Nanocrystal Suspensions. *Langmuir*. 2020;36(32):9551-9561.
49. Tanaka H, Meunier J, Bonn D. Nonergodic states of charged colloidal suspensions: Repulsive and attractive glasses and gels. *Phys Rev E*. 2004;69(3):31404.
50. Solomon MJ, Spicer PT. Microstructural regimes of colloidal rod suspensions, gels, and glasses. *Soft Matter*. 2010;6(7):1391-1400.
51. Kasprzyk-Hordern B. Chemistry of alumina, reactions in aqueous solution and its application in water treatment. *Adv Colloid Interface Sci*. 2004;110(1-2):19-48.
52. Moud AA, Arjmand M, Yan N, Nezhad AS, Hejazi SH. Colloidal behavior of cellulose nanocrystals in presence of sodium chloride. *ChemistrySelect*. 2018;3(17):4969-4978.
53. Chakraborty A, Chakraborty T, Menendez MI, Chattopadhyay T. Surfactant-Mediated Solubilization of Magnetically Separable Nanocatalysts for the Oxidation of Alcohols. *ACS omega*. 2019;4(7):11558-11565.
54. Kim J-Y, Song J-Y, Lee E-J, Park S-K. Rheological properties and microstructures of Carbopol gel network system. *Colloid Polym Sci*. 2003;281(7):614-623.
55. Tiu C, Guo J, Uhlherr PHT. Yielding behaviour of viscoplastic materials. *J Ind Eng Chem*. 2006;12(5):653-662.
56. Uhlherr PHT, Guo J, Tiu C, Zhang X-M, Zhou J-Q, Fang T-N. The shear-induced solid–liquid transition in yield stress materials with chemically different structures. *J Nonnewton Fluid Mech*. 2005;125(2-3):101-119.

57. Shafiei Sabet S. Shear rheology of cellulose nanocrystal (CNC) aqueous suspensions. Published online 2013.
58. Moud AA, Arjmand M, Liu J, Yang Y, Sanati-Nezhad A, Hejazi SH. Cellulose nanocrystal structure in the presence of salts. *Cellulose*. 2019;26(18):9387-9401.
59. Mewis J, Wagner NJ, Thixotropy A. Colloid Interface Sci. 147–148 (2009) 214–227. doi: 10.1016. *J CIS*. 2008;5.
60. Christopoulou C, Petekidis G, Erwin B, Cloitre M, Vlassopoulos D. Ageing and yield behaviour in model soft colloidal glasses. *Philos Trans R Soc A Math Phys Eng Sci*. 2009;367(1909):5051-5071.
61. Lynch JM, Cianci GC, Weeks ER. Dynamics and structure of an aging binary colloidal glass. *Phys Rev E*. 2008;78(3):31410.
62. Folgar F, Tucker III CL. Orientation behavior of fibers in concentrated suspensions. *J Reinf Plast Compos*. 1984;3(2):98-119.
63. Schilling T, Jungblut S, Miller MA. Depletion-induced percolation in networks of nanorods. *Phys Rev Lett*. 2007;98(10):108303.
64. Bauer T, Höfling F, Munk T, Frey E, Franosch T. The localization transition of the two-dimensional Lorentz model. *Eur Phys J Spec Top*. 2010;189(1):103-118.
65. Höfling F, Munk T, Frey E, Franosch T. Critical dynamics of ballistic and Brownian particles in a heterogeneous environment. *J Chem Phys*. 2008;128(16):164517.
66. Dhont JKG, Briels WJ. Viscoelasticity of suspensions of long, rigid rods. *Colloids surfaces A Physicochem Eng Asp*. 2003;213(2-3):131-156.
67. Stover CA, Koch DL, Cohen C. Observations of fibre orientation in simple shear flow of semi-dilute suspensions. *J Fluid Mech*. 1992;238:277-296.
68. Hyun K, Wilhelm M, Klein CO, et al. A review of nonlinear oscillatory shear tests: Analysis and application of large amplitude oscillatory shear (LAOS). *Prog Polym Sci*. 2011;36(12):1697-1753.
69. Dimitriou CJ, Ewoldt RH, McKinley GH. Describing and prescribing the constitutive response of yield stress fluids using large amplitude oscillatory shear stress (LAOStress). *J Rheol (N Y N Y)*. 2013;57(1):27-70.
70. Dinkgreve M, Denn MM, Bonn D. "Everything flows?": elastic effects on startup flows of yield-stress fluids. *Rheol Acta*. 2017;56(3):189-194.
71. Sim HG, Ahn KH, Lee SJ. Large amplitude oscillatory shear behavior of complex fluids

investigated by a network model: a guideline for classification. *J Nonnewton Fluid Mech*. 2003;112(2-3):237-250.

72. Donley GJ, Singh PK, Shetty A, Rogers SA. Elucidating the G ″overshoot in soft materials with a yield transition via a time-resolved experimental strain decomposition. *Proc Natl Acad Sci*. 2020;117(36):21945-21952.
73. Nguyen QD, Boger D V. Measuring the flow properties of yield stress fluids. *Annu Rev Fluid Mech*. 1992;24(1):47-88.
74. Donley GJ, de Bruyn JR, McKinley GH, Rogers SA. Time-resolved dynamics of the yielding transition in soft materials. *J Nonnewton Fluid Mech*. 2019;264:117-134.
75. Chen Y, Xu C, Huang J, Wu D, Lv Q. Rheological properties of nanocrystalline cellulose suspensions. *Carbohydr Polym*. 2017;157:303-310.
76. Larson RG. *The Structure and Rheology of Complex Fluids*. Vol 150. Oxford university press New York; 1999.
77. Falk ML, Langer JS. Dynamics of viscoplastic deformation in amorphous solids. *Phys Rev E*. 1998;57(6):7192.
78. Maloney CE, Lemaître A. Amorphous systems in athermal, quasistatic shear. *Phys Rev E*. 2006;74(1):16118.
79. Schall P, Weitz DA, Spaepen F. Structural rearrangements that govern flow in colloidal glasses. *Science (80-)*. 2007;318(5858):1895-1899.
80. Barnes HA. The yield stress—a review or ‘παντα ρει’—everything flows? *J Nonnewton Fluid Mech*. 1999;81(1-2):133-178.
81. Yoshimura AS, Prud’homme RK. Response of an elastic Bingham fluid to oscillatory shear. *Rheol acta*. 1987;26(5):428-436.
82. Herschel WH, Bulkley R. Konsistenzmessungen von gummi-benzollösungen. *Kolloid-Zeitschrift*. 1926;39(4):291-300.
83. Sollich P, Lequeux F, Hébraud P, Cates ME. Rheology of soft glassy materials. *Phys Rev Lett*. 1997;78(10):2020.
84. Sollich P. Rheological constitutive equation for a model of soft glassy materials. *Phys Rev E*. 1998;58(1):738.
85. Shih WY, Shih W, Aksay IA. Elastic and yield behavior of strongly flocculated colloids. *J Am Ceram Soc*. 1999;82(3):616-624.

86. Yang M, Scriven LE, Macosko CW. Some rheological measurements on magnetic iron oxide suspensions in silicone oil. *J Rheol (N Y N Y)*. 1986;30(5):1015-1029.
87. Mujumdar A, Beris AN, Metzner AB. Transient phenomena in thixotropic systems. *J Nonnewton Fluid Mech*. 2002;102(2):157-178.
88. Divoux T, Barentin C, Manneville S. Stress overshoot in a simple yield stress fluid: An extensive study combining rheology and velocimetry. *Soft Matter*. 2011;7(19):9335-9349.
89. Dinkgreve M, Paredes J, Denn MM, Bonn D. On different ways of measuring "the" yield stress. *J Nonnewton Fluid Mech*. 2016;238:233-241.
90. Ovarlez G, Cohen-Addad S, Krishan K, Goyon J, Coussot P. On the existence of a simple yield stress fluid behavior. *J Nonnewton Fluid Mech*. 2013;193:68-79.
91. Divoux T, Grenard V, Manneville S. Rheological hysteresis in soft glassy materials. *Phys Rev Lett*. 2013;110(1):18304.
92. Mewis J, Spaull AJB. Rheology of concentrated dispersions. *Adv Colloid Interface Sci*. 1976;6(3):173-200.
93. Malkin A, Kulichikhin V, Ilyin S. A modern look on yield stress fluids. *Rheol Acta*. 2017;56(3):177-188.
94. Masalova I, Malkin AY, Foudazi R. Yield stress of emulsions and suspensions as measured in steady shearing and in oscillations. *Appl Rheol*. 2008;18(4):44790-44791.
95. Moghimi E, Petekidis G. Mechanisms of two-step yielding in attractive colloidal glasses. *J Rheol (N Y N Y)*. 2020;64(5):1209-1225.
96. Koumakis N, Laurati M, Egelhaaf SU, Brady JF, Petekidis G. Yielding of hard-sphere glasses during start-up shear. *Phys Rev Lett*. 2012;108(9):98303.
97. Koumakis N, Laurati M, Jacob AR, et al. Start-up shear of concentrated colloidal hard spheres: Stresses, dynamics, and structure. *J Rheol (N Y N Y)*. 2016;60(4):603-623.
98. Siebenbürger M, Ballauff M, Voigtmann T. Creep in colloidal glasses. *Phys Rev Lett*. 2012;108(25):255701.